Hydrol. Earth Syst. Sci. Discuss., https://doi.org/10.5194/hess-2018-443
Manuscript under review for journal Hydrol. Earth Syst. Sci.
Discussion started: 5 September 2018

Hydrology and Earth System Sciences
Discussions

Future evolution and uncertainty of river flow regime change in a deglaciating river basin

Jonathan D Mackay[1,2], Nicholas E Barrand[1], David M Hannah[1], Stefan Krause[1], Christopher R Jackson[2], Jez Everest[3], Guðfinna Aðalgeirsdóttir[4], and Andrew R Black[5]

[1]School of Geography, Earth and Environmental Sciences, University of Birmingham, Edgbaston, Birmingham, B15 2TT, UK
[2]British Geological Survey, Environmental Science Centre, Keyworth, Nottingham, NG12 5GG, UK
[3]British Geological Survey, Lyell Centre, Research Avenue South, Edinburgh, EH14 4AS, UK
[4]Institute of Earth Sciences, University of Iceland, 101 Reykjavík, Iceland
[5]Geography and Environmental Science, University of Dundee, Dundee, DD1 4HN, UK

Correspondence: Jonathan D Mackay (joncka@bgs.ac.uk)

Abstract. The flow regime of glacier-fed rivers are sensitive to climate change due to strong climate-cryosphere-hydrosphere interactions. Previous modelling studies have focussed on projecting changes in annual and seasonal flow magnitude, but neglect other changes in river flow regime that could also have socio-economic and environmental impacts. This study employs a more comprehensive, signature-based analysis of climate change impacts on the river flow regime for the deglaciating Virkisá river basin in southern Iceland. 25 metrics (signatures) are derived from 21st century projections of river flow time-series to evaluate changes in different characteristics (magnitude, timing and variability) of river flow regime over sub-daily to decadal timescales. The projections are produced by a model chain that links numerical models of climate and glacio-hydrology. Five components of the model chain including the emission scenario, numerical climate model, downscaling procedure, snow/ice melt model and runoff-routing model are perturbed to propagate their uncertainties through to the river discharge projections. The signature-based analysis indicates that glacier-fed rivers will exhibit changes in the magnitude, timing and variability of river flows over a range of timescales in response to climate change. For most signatures there is high confidence in the sign of change, but the magnitude of change is uncertain and varies substantially across the different signatures. A decomposition of the projection uncertainties using analysis of variance (ANOVA) shows that all five perturbed model chain components contribute to projection uncertainty, but their relative contributions vary across the signatures (characteristic and timescale) of river flow. Signature-based decompositions of projection uncertainty can be used to better design impact studies to provide more robust projections.

1 Introduction

Mountain watersheds have been referred to as the world's water towers (Viviroli and Weingartner, 2004; Viviroli et al., 2007), partly because they receive large quantities of precipitation relative to adjacent lowlands, but also because they regulate runoff through the seasonal accumulation and melt of snow and ice. The presence of snow and ice profoundly affects characteristics of downstream river flow regime including flow magnitude, timing and variability over a range of timescales (Jansson et al.,

Hydrol. Earth Syst. Sci. Discuss., https://doi.org/10.5194/hess-2018-443
Manuscript under review for journal Hydrol. Earth Syst. Sci.
Discussion started: 5 September 2018

Hydrology and Earth System Sciences
Open Access
EGU
Discussions

2003; Mankin et al., 2015). This is partly due to the periodic (diurnal and seasonal) variations and longer-term (decadal) trends in melt water inputs brought about by fluctuations in glaciological mass balance. In addition, the dynamic water storage and realease properties of snow and ice (runoff-routing) control downstream river flow response to runoff over hourly to seasonal timescales (Willis, 2005). As such, glaciated basins exhibit river flow regimes that differ from their non-glaciated equivalents. For example, the so-called 'compensation effect' has been widely observed in the northern hemisphere, whereby partially-glaciated catchments demonstrate reduced intra-annual flow variability (Fountain and Tangborn, 1985; Chen and Ohmura, 1990).

Mountain glaciers are retreating at unprecedented rates (Zemp et al., 2015) while snow coverage is receding (Vaughan et al., 2013) resulting in observable changes to downstream river flows (Luce and Holden, 2009; Singh et al., 2016; Hernández-Henríquez et al., 2017; Matti et al., 2017). With near-surface air temperature projected to rise over the coming decades (Collins et al., 2013) future changes in river flow regimes in response to cryosphere change could have wide-ranging socio-economic and environmental impacts. Long-term reductions in melt water inputs will disrupt the supply of water available for irrigation (Nolin et al., 2010; McDowell and Hess, 2012; Carey et al., 2014; Baraer et al., 2015). Increased inter-annual and intra-annual flow variability will threaten infrastructure projects such as hydroelectric power stations (Laghari., 2013; Gaudard et al., 2014; Carvajal et al., 2017). The loss of the runoff-regulating effects of snow and ice could result in more frequent short-term very high flows putting downstream populations and infrastructure at risk (Laghari., 2013; Stoffel et al., 2016). Changes in flow magnitude and variability from annual to sub-daily timescales will threaten the sustainability of some of the world's most pristine freshwater ecosystems (Bunn and Arthington, 2002; Naiman et al., 2008; Beamer et al., 2017). Therefore, it is of paramount importance to make reliable projections of changes in downstream river flow regimes from glaciated watersheds so that future impacts can be adapted to and mitigated.

Computational glacio-hydrological models (GHM) driven by numerical climate model (NCM) projections allow us to assess how future river flow regimes will change in glaciated river basins. Past studies have focussed on projecting changes in decadal, annual and seasonal variations in runoff magnitude. Decadal changes in runoff are inevitable over the coming century (e.g. Bliss et al., 2014; Lutz et al., 2014; Shea and Immerzeel, 2016) with many basins already having reached 'peak water' and facing a future of dwindling water supply (Huss and Hock, 2018). Seasonal flow magnitudes are also projected to change as melt cycles evolve and watersheds shift from glacial-nival to pluvial runoff regimes (Kobierska et al., 2013; Duethmann et al., 2016; Ragettli et al., 2016; Garee et al., 2017).

Some studies have projected changes in the magnitude of highest and lowest river flows. Wijngaard et al. (2017) projected an increase in the magnitude of the 10% exceedance flow (Q_{10}) for river basins across the Hindu-Kush-Himalayan region. Similar patterns of change have been shown for the Rhine (Bosshard et al., 2013), upper Indus (Lutz et al., 2016) and Upper Yellow (Vetter et al., 2015) river basins. Stewart et al. (2015) projected a decrease in low flow magnitude (Q_{90}) for the snow-covered Sierra Nevada and Upper Colorado river basins due to shifts in the snowmelt season and changes in precipitation type from snow to rain.

Of course, one could go beyond projecting changes in seasonal to decadal mean flow magnitudes and quantiles of the flow duration curve (FDC). A branch of streamflow analysis that has been widely adopted in hydrology is the calculation of

river flow 'signatures': metrics derived from river discharge time-series that represent different characteristics of river flow over specific timescales. These may include mean flows and FDC quantiles as well as metrics to quantify the variability (e.g. coefficient of variation), timing (e.g. peak flow month) and flashiness (e.g. autocorrelation) of flows. Signatures have been used in the past to analyse catchment runoff behaviour and similarity (Yadav et al., 2007; Ali et al., 2012). Furthermore, their ability to localise specific aspects of runoff behaviour make them ideal diagnostic evaluation metrics for model hypothesis testing (Euser et al., 2013; Coxon et al., 2014; Hrachowitz et al., 2014) and calibration (Hingray et al., 2010; Shafii and Tolson, 2015; Kelleher et al., 2017; Schaefli, 2016). They also offer an opportunity to evaluate past (Sawicz et al., 2014) and future (Casper et al., 2012) river flow regime change. For example, Teutschbein et al. (2015) projected changes in 14 different river flow signatures for 14 snow-covered catchments in Switzerland. They projected changes in daily to annual river flow magnitude, timing and variability, highlighting the breadth of river flow regime sensitivity to climate change. An analysis like this is yet to be undertaken for any glaciated river basins.

Projections of river flow regime are inherently uncertain due to assumptions made about the formulation, parameterisation and boundary conditions of the underlying NCMs (Giorgi et al., 2009) and GHMs (Ragettli et al., 2013; Huss et al., 2014; Jobst et al., 2018). Uncertainties may also be introduced by intermediary steps employed to link the two sets of models together such as downscaling (DS) the NCM output. It is important to quantify the propagation of uncertainties from all sources in the model chain as this provides a basis for assigning more robust levels of confidence to river flow projections. Additionally, one can assess the relative contributions of model chain components to the total projection uncertainty, providing empirical evidence for future research needs (e.g. Meresa and Romanowicz, 2017). Ensemble-based experiments have been used in the past to provide this understanding. Here, different components of the model chain are perturbed, typically using a 'one at a time' (OAT) approach where the spread in projections for each perturbed component is evaluated. Ragettli et al. (2013) perturbed three components of a model chain applied to the Hunza River Basin, northern Pakistan including the NCM structure, statistical DS model and parameterisation of the GHM. They showed that all three sources contributed to annual runoff projection uncertainty, but for the heavily glaciated sub-regions of the catchment, the GHM parameter uncertainty exceeded the effect of other sources. Huss et al. (2014) investigated uncertainty in seasonal river flow projections over the 21st century for the Findelengletscher catchment, Switzerland by modifying the NCM structure, GHM melt model structure and initial ice volume boundary condition. Of these, they found that the NCM structure and initial ice volume were most important while the melt model structure was of secondary importance. Jobst et al. (2018) investigated uncertainties in 21st century river flows at the Clutha river basin, New Zealand. They evaluated contributions from emission scenario (ES), NCM structure, statistical DS approach and melt model structure. Similarly to Huss et al. (2014), they found that NCM structure dominated total projection uncertainty.

The OAT method provides a useful first-order approximation of the relative contribution of each component to the total projection uncertainty. However, findings are dependent on how the non-perturbed model components are fixed. Furthermore, this approach cannot resolve interactions between model components which may also contribute to projection uncertainty (Pianosi et al., 2016). An alternative approach that addresses these shortcomings is the Analysis of Variance (ANOVA) statistical method (von Storch and Zwiers, 1999; Tabachnick and Fidell, 2014). ANOVA has been adopted in a number of recent large basin-scale

Hydrol. Earth Syst. Sci. Discuss., https://doi.org/10.5194/hess-2018-443
Manuscript under review for journal Hydrol. Earth Syst. Sci.
Discussion started: 5 September 2018

Hydrology and Earth System Sciences
Discussions

and global-scale hydrological modelling studies (Bosshard et al., 2013; Addor et al., 2014; Giuntoli et al., 2015; Vetter et al., 2015; Samaniego et al., 2017; Vetter et al., 2017; Yuan et al., 2017) and used to compare uncertainties stemming from ES, NCM, GHM structure and DS approach. While uncertainties associated with future climate tend to dominate projections of future river flows, glaciated catchment projections have shown to be uniquely sensitive to GHM structure (Addor et al., 2014; Giuntoli et al., 2015), particularly in relation to high flows (Vetter et al., 2017). Furthermore, the contribution of projection uncertainty from interactions between model chain components can exceed individual components (Bosshard et al., 2013; Addor et al., 2014; Vetter et al., 2015). Several issues not considered in these studies, however, are yet to be addressed. Firstly, none have investigated a full range of characteristic changes in river flow regime covering decadal to sub-daily timescales. Second, all have incorporated GHM uncertainty using multiple GHM codes, each with their own unique set of process representations, resolution, timestep and climate interpolation strategies making it difficult to determine which model components contribute most to projection uncertainty. Finally, none included a fully integrated mass-conserving, dynamic glacier evolution model component and therefore could not fully account for atmopshere-cryosphere-hydrosphere feedbacks.

This study uses a NCM-DS-GHM model chain to simulate the impact of 21st century climate change on the downstream river flow regime in the deglaciating Virkisá river basin in southern Iceland. Five different components of the model chain are perturbed to represent uncertainty of future ES, NCM structure, statistical DS parameterisation and structure-parameterisation of two primary controls on river flow regime in the GHM: melt and runoff-routing processes. The study has two principal aims: i) to determine how climate change and consequent cryospheric change will impact on downstream river flow regime over the 21st century; and ii) to use ANOVA to quantify the relative influence of the five model chain components to projection uncertainty across the different characteristics of river flow regime. This study addresses each of the aforementioned gaps in previous work. Firstly, changes in river flow regime are assessed quantitatively using 25 river discharge signatures which define different characteristics of river flow regime over a range of timescales. Second, a single, consistent, GHM code is used that can incorporate different model structures and parameterisations of melt and runoff-routing processes allowing for uncertainty stemming from these to be localised. Finally, a fully integrated mass-conserving, dynamic glacier evolution routine is included in the GHM code.

2 Methodology

2.1 Study site

The Virkisá river basin covers an area of 22 km^2 on the western side of the ice-capped Öræfajökull stratovolcano in south-east Iceland (Figure 1) and forms a primary drainage channel for accumulating ice at the mountain summit ($\sim$ 2000 m asl). The glacier flows in a south-westerly direction (average ice surface slope = 0.25) along two distinct glacier arms, Virkisjökull and Falljökull, (hereafter referred to as Virkisjökull) around a bedrock ridge before meeting again at the terminus ($\sim$ 150 m asl). Virkisjökull currently covers $\sim$ 60% of the river basin area, but has been in a phase of retreat since 1990. Between 1990 and 2011 Virkisjökull lost $\sim$ 0.3 km^3 of ice and retreated $\sim$ 0.5 km. A small proglacial lake at the terminus forms the headwater of the Virkisá River. The Virkisá flows through an 800 m bedrock-controlled section flanked on either side by push moraines

Hydrol. Earth Syst. Sci. Discuss., https://doi.org/10.5194/hess-2018-443
Manuscript under review for journal Hydrol. Earth Syst. Sci.
Discussion started: 5 September 2018

Hydrology and Earth System Sciences
Discussions
Open Access
EGU

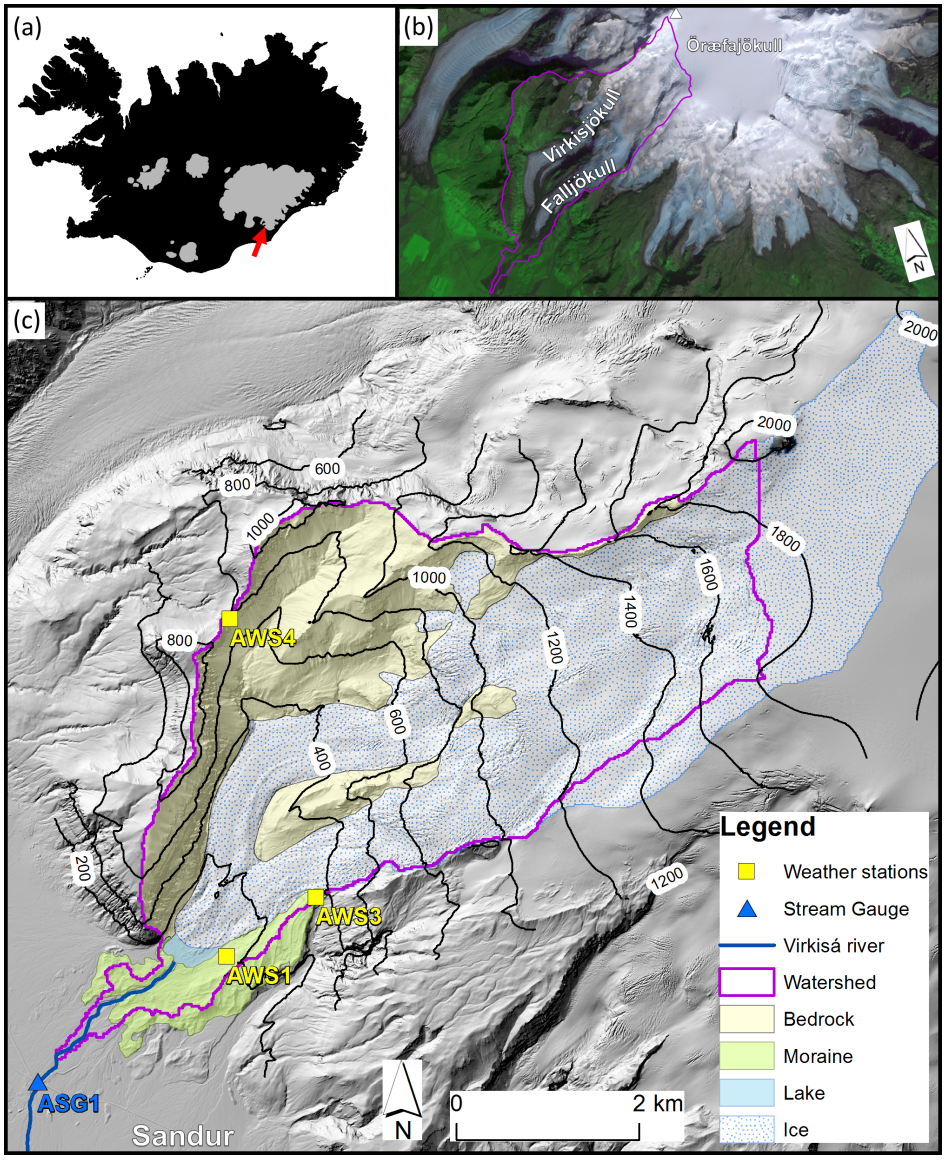

Figure 1. Location of Virkisá river basin in Iceland with glaciated areas highlighted in grey (a); on Öræfajökull (b); and detailed topographical map of basin including major land surface types and meteorological and stream gauging stations (c).

and then over the Skeiðarársandur floodplain typically comprising unconsolidated glacial outwash sediment. The steep-sided valley walls and glacial activity only allow for sporadic development of thin soils with limited vegetation including mosses, grass and shrubs.

The local climate is characterised by cool summers (~ 10 °C on average at the terminus) and mild winters (~ 1 °C on average at the terminus) with an average temperature lapse rate of -0.44 °C 100 m^{-1} (Flett, 2016). There is a significant lateral

precipitation gradient with more than double the annual precipitation falling to the east of Öræfajökull (3500 mm yr^{-1}) than to the west (1500 mm yr^{-1}), an artefact of the prevailing north-easterly winds and orographic effects.

2.2 Climate data

2.2.1 Historical climate

Historical climate data were available from 1981 to 2016 inclusive. A detailed description of these is provided by Mackay et al. (2018). For brevity, only a summary of these data are provided here. The historical climate data include continuous hourly near-surface air temperature and incident solar radiation from automatic weather station 1 (AWS1 in Fig. 1c). A seasonally variable hourly lapse rate was used to extrapolate near-surface air temperature across the study region and an on-ice temperature correction function (Shea and Moore, 2010) was employed to account for katabatic cooling of air in the glacier valleys. For precipitation, the 2.5 km gridded hourly total precipitation data produced as part of the ICRA atmospheric reanalysis project were used, which are currently considered the most accurate gridded precipitation product over Iceland (Nawri et al., 2017). These were bias-corrected against the AWS precipitation data using the equidistant quantile mapping approach (Li et al., 2010).

2.2.2 Regional climate projections

Future climate time-series to 2100 were constructed using the regional climate projections from the Coordinated Regional Climate Downscaling Experiment (CORDEX) (Giorgi et al., 2009). The CORDEX projections are based on an ensemble of regional climate models (RCMs) driven by global circulation model (GCM) simulations from the latest Coupled Model Intercomparison Project (CMIP5) (Taylor et al., 2012). Iceland is covered by the EURO-CORDEX and ARCTIC-CORDEX regional model domains. Following the review by Gosseling (2017), the EURO-CORDEX data were used as these include projections at a higher 0.11° spatial resolution and a larger ensemble of GCM-RCM combinations allowing better exploration of climate model uncertainty.

The 0.11° EURO-CORDEX simulations span the years 1950-2100 with simulations up to 2005 constituting the 'recent past' where influences such as atmospheric composition, solar forcing and emissions are imposed based on observations. From 2006, three future ESs or Representative Concentration Pathways (RCP) were imposed on the models including RCP2.6, RCP4.5 and RCP8.5 which represent an additional radiative forcing by 2100 relative to pre-industrial values of +2.6, +4.5 and +8.5 W m^{-2} respectively. All simulations are available at 3-hourly to 3-monthly resolution, however the 3-hourly simulations were only produced using 4 GCM-RCMs while daily to seasonal simulations were produced using 15. Given the intent of this study to analyse projection uncertainty, it was decided that the daily data were most suitable. The RCP2.6 ES was omitted from the model experiments as only 8 of 15 GCM-RCMs within the CORDEX archive were forced with this. Furthermore, the probability of achieving the RCP2.6 targets is increasingly unlikely (Sanford et al., 2014; Fyke and Matthews, 2015) and arguably completely infeasible (Mora et al., 2013) given the current global emission trajectory.

GCM-RCM skill was analysed by comparing the empirical distribution functions (ECDFs) of the daily catchment-average historical observation climate data and the GCM-RCM simulations for the recent past (1981 - 2005). While the skill was vari-

able across the GCM-RCMs, one was consistently poor across all three climate variables (GCM:CNRM-CM5, RCM:CNRM-ALADIN53). Accordingly, this GCM-RCM was removed from the climate model ensemble. Figure 2 shows the simulated ECDFs from the 14 remaining GCM-RCMs for four months of the year (January, April, July and October). Overall, the GCM-RCM performance is good, broadly capturing the seasonal change in the ECDFs, however some biases are notable. In particular, the highest precipitation events are generally overestimated and there is a clear positive bias in the incident solar radiation simulations. Conversely, temperature shows some negative bias, particularly for the coldest days in January and April.

2.2.3 Downscaling regional climate projections

The statistical delta-change downscaling approach was employed which has been widely applied in hydrological impact studies (Farinotti et al., 2012; Immerzeel et al., 2013; Kobierska et al., 2013; Huss et al., 2014; Lutz et al., 2016). While most studies have used monthly mean delta-change values to capture seasonal shifts in climate, several recent investigations have used advanced quantile-based approaches which account for changes in higher-order statistical properties of future climate by evaluating shifts in the ECDFs of climate variables. Including these higher-order changes has shown to be important for evaluating shifts in extreme high flows and sub-seasonal metrics of river flow projections (Jakob Themeßl et al., 2011; Immerzeel et al., 2013; Lutz et al., 2016). In addition, shifts in the day-to-day variability of temperature impact projections of glacier retreat as these variations control the periodic rising of temperature above the melting point (Beer et al., 2018). Accordingly, the advanced delta-change approach was adopted in this study. The approach is summarised in five steps which were applied to each combination of GCM-RCM, climate variable and ES separately:

1. The climate variable time-series was divided into four 25-year long periods including the recent past (1981 - 2005) and early (2006 - 2030), mid (2041-2065) and late (2076 - 2100) 21st century.

2. For each of the four periods, all daily data points were further divided into 12 sub-samples representing each month of the year. An ECDF was constructed for each month of each period.

3. For each month of each future period, ten deltas were calculated by taking the mean difference between the recent past and future ECDF for each 10% section (see grey bars in Fig. 3a for example).

4. Given the need for transient climate time-series to simulate glacier evolution over the 21st century, a daily delta time-series from 2006 to 2100 was constructed for each ECDF section of each month by linearly interpolating between the calculated deltas of each future period (e.g. as implemented by Farinotti et al., 2012), using the midpoints of the future periods as interpolation points (Figure 3b).

5. The hourly historic observation data for the recent past were randomly sampled on a year-by-year basis to generate an initial unperturbed future climate variable time-series (blue dash, Fig. 3c). The daily deltas were applied to this time-series for each month and ECDF section separately to generate a future perturbed climate time-series at an hourly resolution (orange dash Fig. 3c).

Hydrol. Earth Syst. Sci. Discuss., https://doi.org/10.5194/hess-2018-443
Manuscript under review for journal Hydrol. Earth Syst. Sci.
Discussion started: 5 September 2018

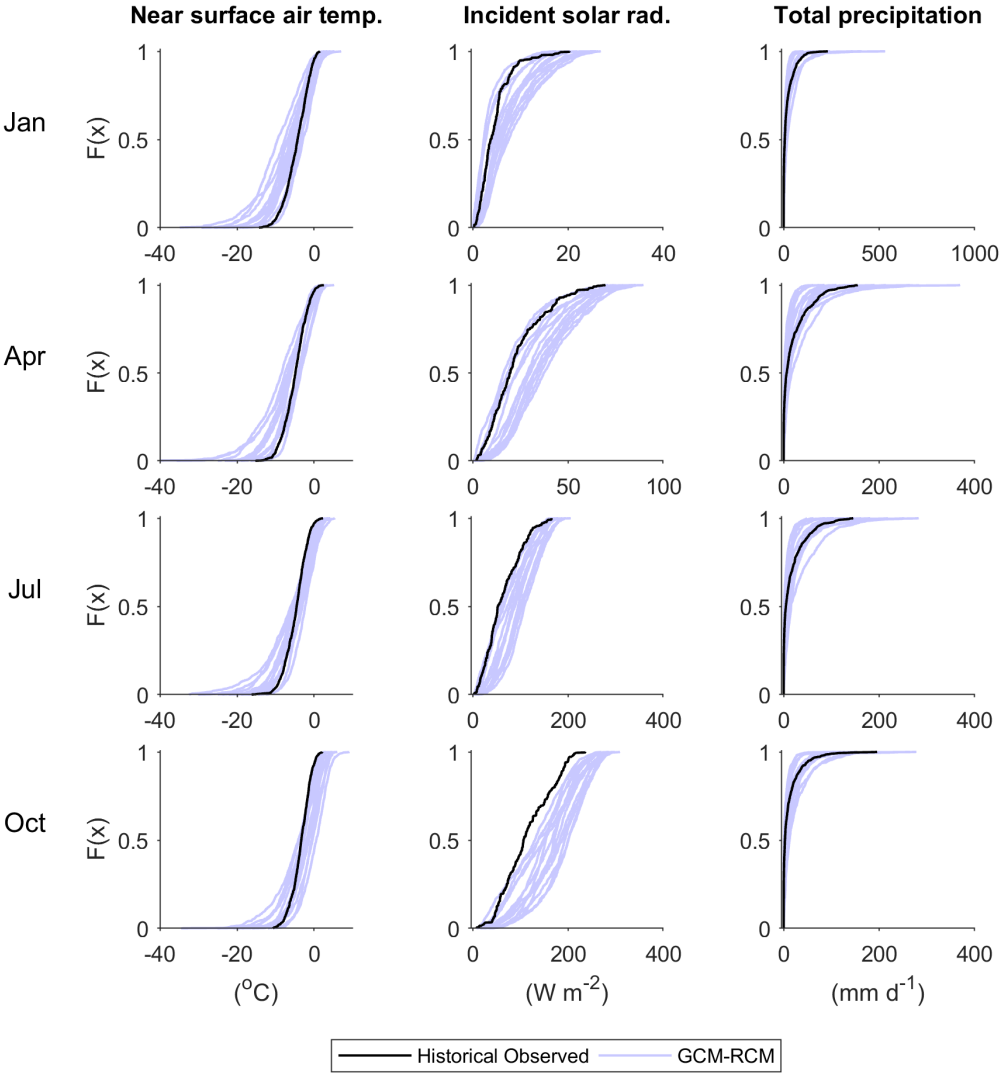

Figure 2. Comparison of daily catchment-average observed and simulated (14 GCM-RCMs) monthly ECDFs for the recent past (1981-2005) for the months of January, April, July and October.

Hydrol. Earth Syst. Sci. Discuss., https://doi.org/10.5194/hess-2018-443
Manuscript under review for journal Hydrol. Earth Syst. Sci.
Discussion started: 5 September 2018

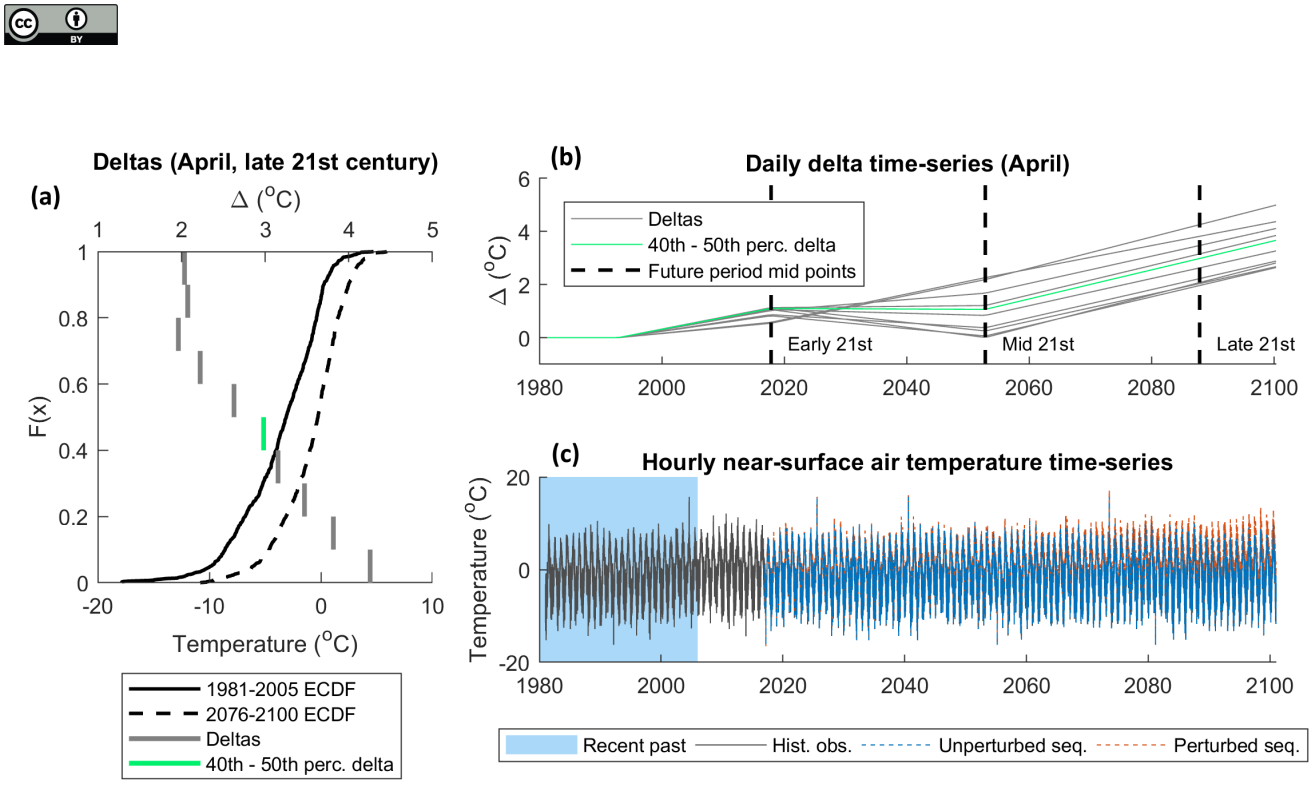

Figure 3. Example of advanced delta-change approach when applied to near surface air temperature data based on the projections from 1 of the 14 GCM-RCMs with the RCP8.5 ES. Deltas (grey bars) derived from ECDFs (black curves) for April in late 21st century (a); Daily delta time-series for each section of the April ECDFs (green line represents 40th - 50th percentile section) (b); Initial and perturbed future temperature time-series when deltas for all months and ECDF sections are applied (c).

For temperature, catchment average daily deltas were applied evenly across the catchment and each daily period of the unperturbed time-series. Accordingly, diurnal temperature variability and lapse rates were assumed not to change in the future. For incident solar radiation and precipitation, proportional deltas were used to prevent negative values and preserve the sub-daily proportional distribution of these variables in space and time.

It was noted upon visual inspection, that the inter-annual variability of the future climate time-series was very sensitive to the random sampling of the historic climate data (step 5 above). Accordingly, uncertainty associated with this aspect of the DS parameterisation was considered by using ten different random historic climate samples. As such a total of 2 ES × 14 GCM-RCM × 10 DS parameterisations = 280 future climate time-series were generated for this study.

2.3 Glacio-hydrological model

The distributed GHM code implemented by Mackay et al. (2018) was used in this study because it includes a dynamic, mass-conserving glacier evolution component and also allows the user to utilise different model structures of melt and runoff-routing processes. The GHM resolves glacio-hydrological processes over a regular 2D Cartesian grid of nodes driven by hourly climate data including precipitation, temperature and incident solar radiation. Empirical 'index-based' equations simulate the melt of

Hydrol. Earth Syst. Sci. Discuss., https://doi.org/10.5194/hess-2018-443
Manuscript under review for journal Hydrol. Earth Syst. Sci.
Discussion started: 5 September 2018

Hydrology and Earth System Sciences
Open Access
EGU
Discussions

snow and ice. Snow redistribution by drift and avalanches is calculated using the curvature and slope of the surface (Huss et al., 2008) while the mass-conserving Δh parametrisation of glacier retreat (Huss et al., 2010) resolves changes in the glacier geometry. A soil infiltration and evapotranspiration model (Griffiths et al., 2006) solves the water balance for model nodes with no ice or snow coverage. Excess soil moisture, rainfall and melt are routed to the catchment outlet via a semi-distributed network of linear-reservoir cascades (Ponce, 2014) which represent the average water storage and release characteristics of the major hydrological pathways in the watershed.

The selection of melt and runoff-routing model structures was based on the findings of Mackay et al. (2018). They applied nine different combinations of three melt model structures and three runoff-routing model structures of varied complexity in the GHM and evaluated their ability to capture a range of river discharge signatures derived from observation time-series at automatic stream gauge 1 (ASG1 in Fig. 1c) which has been operational since 2012. They also used observation data of ice melt and snow coverage to derive signatures that described different aspects of these data. They showed that while introducing model complexity did improve simulations when evaluated against specific signatures, it did not necessarily result in better consistency across all signatures, emphasising model selection uncertainty. The most complex runoff-routing structure, however, was consistently the least efficient when compared to the two simpler alternatives, particularly in relation to capturing signatures representing high river flow events. As such, this model structure was discarded, and only the remaining six combinations of melt and runoff-routing models structures were used in this study. These included three melt model structures: i) the classic temperature index model (TIM_1) where melt increases linearly with near surface air temperature above a critical threshold (e.g. Braithwaite, 1995); ii) the enhanced temperature-index model (TIM_2) proposed by Hock (1999) which accounts for topographic effects on incident solar radiation including surface slope, aspect and shading from the surrounding landform; and iii) the enhanced temperature-index model (TIM_3) proposed by Pellicciotti et al. (2005) which accounts for topographic effects and also includes a dynamic snow-albedo parameterisation (Brock et al., 2000) which accounts for the drop in snow albedo as it ages. Each melt model structure was combined with the two runoff-routing structures: i) a single linear reservoir cascade (ROR_1) which routes runoff from all sources (ice melt, snowmelt, rainfall and excess soil water) simultaneously; and ii) two linear reservoir cascades in parallel (ROR_2) where the first represents the slow percolation of water through the snow and firn and the second represents faster flow of water through and over bare ice and overland. The simplest ROR_1 structure assumes all catchment water stores delay and diffuse downstream river response to runoff in the same way, effectively fixing the run-off routing behaviour of the catchment over time. The more complex ROR_2 structure accounts for temporal variations in the drainage efficiency of the catchment according to changes in snow and ice coverage.

2.4 Signatures of river flow regime

Table 1 lists the 25 signatures of river discharge used to evaluate future changes in river flow regime. The majority of signatures were selected from past studies and were chosen to reflect the types of changes that one might expect to see in snow and ice covered catchments. They also broadly follow those used in the model assessment study of Mackay et al. (2018). The signatures are grouped into seven different attributes and further categorised by the characteristic(s) of flow regime that they evaluate and their temporal scale. At the decadal timescale, two signatures were selected. These include the 'peak water', which defines

Hydrol. Earth Syst. Sci. Discuss., https://doi.org/10.5194/hess-2018-443
Manuscript under review for journal Hydrol. Earth Syst. Sci.
Discussion started: 5 September 2018

Hydrology and Earth System Sciences
Discussions

Table 1. Summary of 25 river discharge signatures used to evaluate future changes in river flow regime. Those with available limits of acceptability were also used as part of the GHM calibration and evaluation procedure.

Attribute	Signature	Limits of acceptability		Regime characteristic	Temporal scale
		Calibration (2013-2014)	Evaluation (2015-2016)		
Inter-annual flow	Peak water (PW)	-	-	Timing and magnitude	Decadal
	Inter-annual flow range (R_{ANN})	-	-	Variability	Decadal
Annual river flows	Mean annual river flow ($\bar{Q}$)	-	-	Magnitude	Annual
Monthly river flows	Mean January river flow ($\bar{Q}_{JAN}$)	1.16 – 1.86 $m^3 s^{-1}$	-	Timing and magnitude	Monthly
	Mean February river flow ($\bar{Q}_{FEB}$)	1.69 – 2.92 $m^3 s^{-1}$	-	Timing and magnitude	Monthly
	Mean March river flow ($\bar{Q}_{MAR}$)	0.85 – 1.58 $m^3 s^{-1}$	1.22 - 2.34 $m^3 s^{-1}$	Timing and magnitude	Monthly
	Mean April river flow ($\bar{Q}_{APR}$)	0.73 – 1.48 $m^3 s^{-1}$	1.03 - 2.10 $m^3 s^{-1}$	Timing and magnitude	Monthly
	Mean May river flow ($\bar{Q}_{MAY}$)	1.50 – 2.16 $m^3 s^{-1}$	1.64 - 3.00 $m^3 s^{-1}$	Timing and magnitude	Monthly
	Mean June river flow ($\bar{Q}_{JUN}$)	4.12 – 6.23 $m^3 s^{-1}$	4.88 - 9.39 $m^3 s^{-1}$	Timing and magnitude	Monthly
	Mean July river flow ($\bar{Q}_{JUL}$)	6.33 – 10.3 $m^3 s^{-1}$	4.96 - 9.38 $m^3 s^{-1}$	Timing and magnitude	Monthly
	Mean August river flow ($\bar{Q}_{AUG}$)	5.72 – 9.15 $m^3 s^{-1}$	6.80 - 14.39 $m^3 s^{-1}$	Timing and magnitude	Monthly
	Mean September river flow ($\bar{Q}_{SEP}$)	4.55 – 7.38 $m^3 s^{-1}$	6.61 - 14.21 $m^3 s^{-1}$	Timing and magnitude	Monthly
	Mean October river flow ($\bar{Q}_{OCT}$)	3.88 – 7.02 $m^3 s^{-1}$	6.94 - 16.33 $m^3 s^{-1}$	Timing and magnitude	Monthly
	Mean November river flow ($\bar{Q}_{NOV}$)	3.90 – 7.40 $m^3 s^{-1}$	3.17 - 5.76 $m^3 s^{-1}$	Timing and magnitude	Monthly
	Mean December river flow ($\bar{Q}_{DEC}$)	-	-	Timing and magnitude	Monthly
	Mean monthly flow range (R_{mnth})	-	-	Variability	Seasonal
Slow release low flows	95% exceedance flow (Q_{95})	0.27 - 1.10 $m^3 s^{-1}$	0.66 - 1.75 $m^3 s^{-1}$	Magnitude	Monthly to seasonal
	99% exceedance flow (Q_{99})	0.12 - 0.88 $m^3 s^{-1}$	0.46 - 1.56 $m^3 s^{-1}$	Magnitude	Monthly to seasonal
	Low flow standard deviation ($\sigma_{99\text{-}95}$)	0.03 - 0.10 $m^3 s^{-1}$	0.02 - 0.09 $m^3 s^{-1}$	Variability	Monthly to seasonal
Moderate flows	50% exceedance flow (Q_{50})	2.38 - 3.70 $m^3 s^{-1}$	3.10 - 5.79 $m^3 s^{-1}$	Magnitude	Daily to monthly
	Moderate flow standard deviation ($\sigma_{52\text{-}48}$)	0.07 - 0.15 $m^3 s^{-1}$	0.08 - 0.18 $m^3 s^{-1}$	Variability	Daily to monthly
Quick release high flows	1% exceedance flow (Q_{01})	17.71 - 40.31 $m^3 s^{-1}$	21.90 - 61.57 $m^3 s^{-1}$	Magnitude	Hourly to daily
	5% exceedance flow (Q_{05})	9.43 - 15.76 $m^3 s^{-1}$	11.71 - 27.37 $m^3 s^{-1}$	Magnitude	Hourly to daily
	High flow standard deviation ($\sigma_{05\text{-}01}$)	2.08 - 5.68 $m^3 s^{-1}$	2.60 - 8.10 $m^3 s^{-1}$	Variability	Hourly to daily
Flashiness	Integral scale (τ)	25 – 44 hr	0 - 54 hr	Timing	Hourly to daily

the timing (by year) of maximum flow, as well as the inter-annual flow range which characterises long term flow variability. Changes in mean annual river flow were also evaluated, while mean monthly flows were used to evaluate changes to the seasonal timing and magnitude of river flow. The range in mean monthly flows was also chosen to evaluate intra-annual flow variability. In addition, eight signatures were selected which broadly describe the magnitude and variability of slow release low flows (99-95% exceedance flows), moderate flows (52-48% exceedance) and quick release high flows (5-1% exceedance). For these, the quantiles of the FDC were used to assess changes in the magnitude of these flow types. The standard deviation was also used to define flow variability of each flow type. Finally, the integral scale, which measures the lag time at which the autocorrelation function of the river flow time-series falls below $\frac{1}{e}$ was utilised as an indicator of the response time of the catchment to runoff events (flashiness).

2.5 GHM calibration

Given the focus on projecting changes in river discharge signatures, these were explicitly included in the GHM calibration procedure as this gives better signature simulations than using traditional global objective functions (Kiesel et al., 2017; Pool

Hydrol. Earth Syst. Sci. Discuss., https://doi.org/10.5194/hess-2018-443
Manuscript under review for journal Hydrol. Earth Syst. Sci.
Discussion started: 5 September 2018

Hydrology and Earth System Sciences
Discussions

et al., 2017). Calibrating against river flow data alone can lead to unrealistic snow and glacier melt rates, inhibiting model consistency and increasing projection uncertainties (Konz and Seibert, 2010; Finger et al., 2011; Schaefli and Huss, 2011; Hanzer et al., 2016). Accordingly, a novel signature-based calibration of the GHM was undertaken by evaluating the GHM against 20 of the river discharge signatures in Table 1 for which observation data exists calculated from hourly river discharge measurements (Macdonald et al., 2016) at the automatic stream gauge (ASG1 in Fig. 1) in combination with 12 signatures of ice melt and snow coverage (Appendix A).

For each signature, model simulations were compared to observations using a continuous acceptability score that is analogous to those used in other signature-based hydrological studies (Coxon et al., 2014; Shafii and Tolson, 2015). This objective function explicitly accounts for uncertainty in the observation signatures, hereafter termed 'limits of acceptability' (LOA), so that decisions about model appropriateness can be made within the uncertainties of observation data. In this study the 95% confidence bounds were used to define the LOA for the river discharge signatures (Table 1) and the ice melt and snow coverage signatures (Table A1). Details of how these were derived can be found in the study of Mackay et al. (2018). The acceptability for signature j is defined as:

$$s_j = \begin{cases} 0 & low_j \leq sim_j \leq upp_j \\ \frac{sim_j - upp_j}{upp_j - obs_j} & sim_j > upp_j \\ \frac{sim_j - low_j}{obs_j - low_j} & sim_j < low_j \end{cases} \quad (1)$$

where obs_j and sim_j are the observed and simulated values and upp_j and low_j are the upper and lower LOA. A score of zero indicates that the model captures the signature within the LOA. A non-zero score is given for any simulation that falls outside of the LOA with a sign that indicates the direction of bias and a magnitude that indicates the model's performance relative to the LOA. A score of -3 would indicate that the model underestimates the signature by three times the observation uncertainty. This score therefore does not penalise a model if it falls within the observation uncertainty of a signature. It is also tolerant of projections that fall outside of the LOA where observation uncertainty is high; a desirable attribute given the range of signatures the GHM was evaluated against.

The aim of the calibration was to extract an ensemble of GHM compositions (TIM and ROR structure-parameter combinations) that were most acceptable across the river discharge signatures whilst broadly reproducing the snow coverage and ice melt signatures. This was achieved using a three-stage Monte-Carlo procedure which was devised so that the resultant GHM ensemble reflected the uncertainty in model selection given the known inconsistencies of the GHM across the signatures.

2.5.1 Stage 1: TIM calibration

The first stage aimed to extract the optimal TIM compositions (structure-parameter combinations) by calibrating them against the 12 snow coverage and ice melt signatures. Here, for each of the three TIM structures, 5000 TIM parameter sets were drawn from pre-defined uniform distributions (Table B1) using the quasi-random Sobol sampling strategy (Brately and Fox, 1988) to sample the parameter space as efficiently as possible. For each parameter set, the GHM was spun-up for three years from 1985

to 1988 with a static ice geometry fixed to a 1988 ice DEM (Magnússon et al., 2016). The GHM was then run from 1988 to the end of 2016 with a freely evolving glacier geometry.

Given the high degree of glaciation in the study catchment, and its recent rapid retreat, an initial emphasis of the calibration was put on the model's ability to capture the long term glacier volume change signature. Accordingly, only those TIM compositions that captured this signature within the LOA were considered and the rest were discarded. These remaining compositions were then further refined by evaluating them against the remaining 11 snow and ice signatures. First, the TIM compositions were sorted by structure (TIM_1,TIM_2,TIM_3). Then, for a given TIM structure, the following steps were applied:

1. Find the TIM parameter set(s) that capture the signature within the LOA and discard the rest. If more than one parameter set captures the current signature, go to step 2. If none capture the current signature, discard none and go to step 2.

2. Of the remaining models, find that which best captures the 11 remaining snow and ice signatures overall according to the weighted mean scores obtained in Eq. 1. The weights were applied to ensure that equal preference was given to ice melt and snow coverage signatures.

24 unique TIM compositions were obtained from this calibration stage made up of eight unique parameterisations of each of the three TIM structures. In some cases the same composition was selected more than once which was accounted for by weighting the simulations in the results presented throughout this study.

2.5.2 Stage 2: ROR calibration

The second calibration stage aimed to extract the optimal ROR compositions when used in combination with the 24 pre-selected TIM compositions by calibrating them against 20 of the river discharge signatures obtained from observations of river discharge for the years 2013 and 2014 (see signatures with calibration LOA in Table 1). Note, the inter-annual flow signatures and the mean December river flow signatures could not be calculated as there was insufficient observation data. Furthermore, the mean annual river flow and mean monthly flow range were not included as this information was already accounted for in the mean monthly flow signatures. Here, 5000 random ROR parameter sets were drawn for each ROR structure. Each was used in combination with the pre-selected TIM compositions in the GHM. Then, the two steps outlined in calibration stage 1 were applied using the 20 calibration river discharge signatures with two notable differences. Firstly, for each ROR structure and each river discharge signature, rather than selecting a unique ROR parameter set for each of the 24 TIM compositions, a single parameter set was selected based on its mean performance across the 24 TIM compositions. This was done to satisfy the ANOVA requirements so that the TIM and ROR composition uncertainty could be analysed separately. Furthermore, for step 2, the signatures were weighted so that each of the attributes in Table 1 were weighted equally. In total, 14 unique ROR compositions were selected made up of seven unique parameterisations of the ROR_1 and ROR_2 structures, giving a total of $24 \times 14 = 336$ unique GHM compositions.

2.5.3 Stage 3: Evaluation of calibrated GHM compositions

After calibration, the simulated river discharge time-series and signatures were evaluated against river discharge observations covering the years 2015 and 2016. Note, no data for mean January and February flows were available for these years. Figures 4a and b show the simulated 'capture ratio' (the ratio of the 336 GHM compositions that capture the observation data within their 95% uncertainty bounds) time-series projected onto the mean observed river discharge for the years 2015 and 2016 respectively. Also shown is the ensemble mean simulated river discharge (black dash) which while not indicative of a single GHM simulation, does provide an indication of overall projection bias.

56% of the observation time-series were captured by at least half of the GHM compositions, while 41% and 28% of the observations were captured by at least 75% and 90% of the GHM compositions. 12% of the observations were not captured by any of the GHM compositions. These included some of the low flows observed at the beginning of the year outside of the melt season, particularly in 2015, where the GHM showed consistent negative biases. Some rainfall-induced summer peak flows were also not captured, particularly during the late summer months of August and September. Furthermore, the sustained summer melt runoff discharge in between rainfall-induced peak flows tended to be overestimated (for example during July and August 2016). Even so, the flow duration curve (FDC) in Fig. 4c shows that almost the entire FDC was captured by all of the GHM simulations except for some of the lowest flows on record. Indeed, Fig. 4d reveals that GHMs were least efficient at capturing the low flow signatures, particularly the variability signature ($\sigma_{99\text{-}95}$), where simulations were positively biased by almost four times the observation uncertainty. For the remaining signatures though, the ensemble of GHMs were remarkably efficient, with the majority of simulations (and in most cases all of them) capturing these signatures within their 95% observation uncertainty bounds.

2.6 21st century projections

For the 21st century runs, all 336 GHM compositions were run to the end of 2016 using the historic observed climate to capture the evolving ice geometry as accurately as possible. From 2017 to 2100, the 280 downscaled future climate time-series were used to drive the GHM compositions resulting in 94080 individual model chain runs. Prior to running the full ensemble, a preliminary subset of 2000 runs from the ensemble was run for the 21st century to ensure the model chain was behaving as expected. From these it was found that ~5% of the runs simulated sustained positive glacier mass balance over the future period. Given that the Δh glacier evolution parametrisation is not designed to simulate glacier advance, these simulations resulted in an unrealistic build up of ice at the glacier tongue without any simulated areal advance of the glacier. Recently, Seibert et al. (2018) presented an implementation of the original Δh parameterisation that provides more realistic simulations of glacier evolution under periods of sustained positive mass balance. They propose running the Δh parametrisation a priori outside of the GHM. A small negative mass balance is used to force the Δh model from an initial glacier profile (ideally its maximum observed extent) until the glacier has disappeared completely. At each step, the glacier mass and geometry are stored in the form of a lookup table. On running the GHM, the retreat/advance of the glacier is derived from the lookup table as a function of the simulated glacier mass.

Hydrol. Earth Syst. Sci. Discuss., https://doi.org/10.5194/hess-2018-443
Manuscript under review for journal Hydrol. Earth Syst. Sci.
Discussion started: 5 September 2018

Hydrology and Earth System Sciences
Discussions

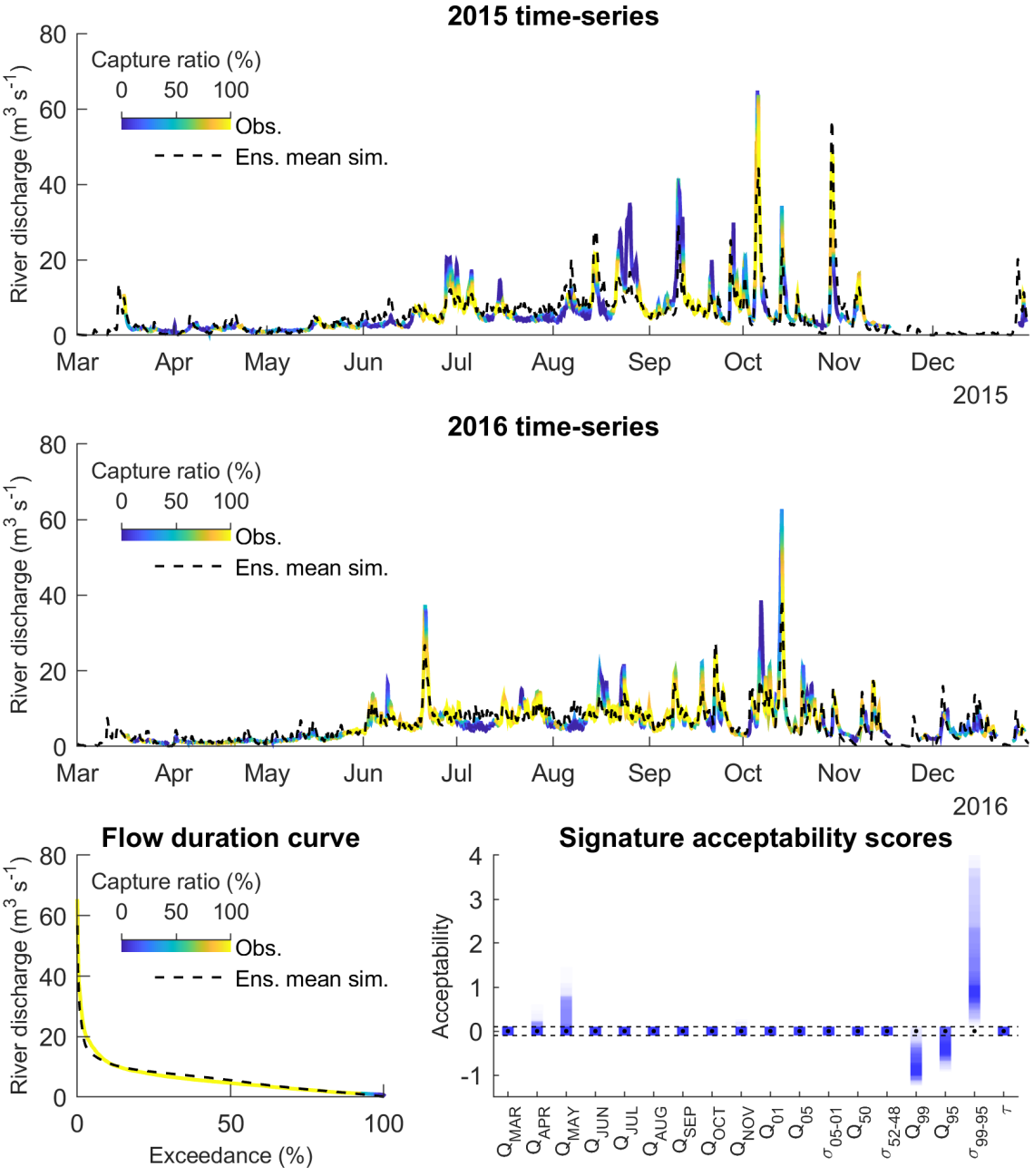

Figure 4. Capture ratio projected onto observed river discharge data during evaluation period for 2015 (a); 2016 (b); and over the FDC (c). The weighted ensemble mean simulation is shown as a black dash. Also shown are the range of acceptability scores for each of the available river discharge signatures over the evaluation period (d). Acceptable simulations in (d) are those contained within the black dash lines.

Hydrol. Earth Syst. Sci. Discuss., https://doi.org/10.5194/hess-2018-443
Manuscript under review for journal Hydrol. Earth Syst. Sci.
Discussion started: 5 September 2018

Seibert et al. (2018) note that this approach neglects any delays in the response of glacier advance to mass balance changes and is also limited to advancing the glacier as far as the maximum observed glacier extent. It should also be noted that the use of a 'static' lookup table modifies the behaviour of the Δh formulation during periods of retreat. In the original formulation three consecutive years of -1 m w.e. surface mass balance would not necessarily produce the same glacier geometry as a single year of -3 m w.e. for example. This is because of the non-linear structure of the Δh polynomial that defines the relationship between mass balance and glacier geometry. The simulated glacier geometry after a period of time is thus dependent on the cumulative mass balance and the annual sequencing of mass balance. The approach proposed by Seibert et al. (2018) only accounts for the former. Accordingly, a modified implementation of the Seibert et al. (2018) approach was used in this study. Here, the original Δh formulation was used for periods of negative glacier mass balance. The GHM was then modified so that for each simulation year, the simulated glacier mass and geometry were stored in memory. If a positive glacier mass balance (ΔM) was simulated, the GHM would log the current glacier mass ($M_{current}$) and then look for the most recent historical simulated glacier mass (M_{hist}) that exceeded $M_{current} + \Delta M$. The Δh model was then run with a negative mass balance (ΔM^*) so that $M_{hist} + \Delta M^* = M_{current} + \Delta M$. This approach therefore behaves like the original Δh formulation during periods of glacier retreat and allows for the simulation of glacier advance while accounting for mass balance sequencing effects on the model behaviour.

On running the full ensemble, it was found that <2% of the simulations showed periods of glacier advance of more than five consecutive years.

2.7 ANOVA uncertainty analysis

For each model chain run, projections of watershed snow and ice coverage and the 25 river discharge signatures were extracted for each decade from the 1990s (1991-2000) to the 2090s (2091-2100). Future changes in these were then calculated using the 1990s as the reference period and the eight decades influenced by future climate change (2020s to 2090s) as the change periods. The 1990s was chosen as the reference period given that the glacier extent was near its maximum and relatively stable over this period. Note, the peak water (PW) signature can only be calculated taking into account the full projection time-series and as such, it was not possible to apply ANOVA to decadal metrics of change for this signature. ANOVA was used to quantify the effect size of the five components of the model chain, hereafter termed *factors*, on each decadal projection of change. The five factors include the 2×future ES, 14×GCM-RCM combinations, 10×DS parameterisations, 24×TIM compositions and 14×ROR compositions. ANOVA offers an intuitive approach to estimate the effect size of each factor on each signature by partitioning the total sum of squares (SS_{tot}) in the response variable over all combinations of factor levels:

$$SS_{tot} = SS_a + SS_b + SS_c + SS_d + SS_e + SS_I + SS_\varepsilon \tag{2}$$

where:

$$SS_{tot} = \sum_{i=1}^{n_a}\sum_{j=1}^{n_b}\sum_{k=1}^{n_c}\sum_{l=1}^{n_d}\sum_{m=1}^{n_e}(y_{i,j,k,l,m} - \bar{Y})^2 \tag{3}$$

Hydrol. Earth Syst. Sci. Discuss., https://doi.org/10.5194/hess-2018-443
Manuscript under review for journal Hydrol. Earth Syst. Sci.
Discussion started: 5 September 2018

Hydrology and Earth System Sciences
Discussions

where n_a, n_b, n_c, n_d and n_e are the number of levels for each factor, y is the response for a given treatment (i.e. combination of factor levels) and $\bar{Y}$ is the grand mean of the response variable over all treatments. SS_a, SS_b, SS_c, SS_d and SS_e in Eq. 2 are the sum of squares due to the main effects, i.e. the variability in the response variable due to varying a given factor on its own. For example:

$$SS_a = n_b n_c n_d n_e \sum_{i=1}^{n_a} (y_{i,\circ,\circ,\circ,\circ} - \bar{Y})^2 \tag{4}$$

where $\circ$ indicates averaging over an index. SS_I includes all non-additive interaction terms where the combined effect of two or more factors is not the sum of their main effects. For a 5-factor ANOVA, one could include all unique n-tuple combinations of factors where $n = (2,3,4,5)$. Given the difficulty in interpreting these higher-order interactions, and computational requirements, it was decided to investigate the nine first-order interactions only, so that:

$$SS_I = SS_{ab} + SS_{ac} + SS_{ad} + SS_{ae} + SS_{bc} + SS_{bd} + SS_{be} + SS_{cd} + SS_{ce} + SS_{de} \tag{5}$$

The sum of squares for a first-order interaction are calculated as follows using factors a and b as an example:

$$SS_{ab} = n_c n_d n_e \sum_{i=1}^{n_a} \sum_{j=1}^{n_b} (y_{i,j,\circ,\circ,\circ} - y_{i,\circ,\circ,\circ,\circ} - y_{\circ,j,\circ,\circ,\circ} + \bar{Y})^2 \tag{6}$$

Finally, the SS_ε term includes all unexplained variance i.e. error in the ANOVA model.

Having partitioned the sum of squares, the effect size, η^2 for any term in Eq. 3 can be taken as the proportion of the total sum of squares:

$$\eta_*^2 = SS_* / SS_{tot} \tag{7}$$

where $*$ can be any of the main effects, interactions or error term.

Bosshard et al. (2013) showed that because ANOVA is based on a biased variance estimator that underestimates the variance in small sample sizes, the calculated effect sizes are biased if a different number of levels are used for each factor. Given that the number of factor levels range from 2 to 24, a pure application of ANOVA using all possible treatments would lead to biased results. Bosshard et al. (2013) outlined a method to correct for this which involves sub-sampling the factor levels down to the smallest number levels across all factors. The procedure is repeated using every possible combination of factor levels with unbiased effect size taken as the mean across all sub-samples. However, given that there are $C(94080, 2) \approx 4 \times 10^9$ unique combinations of factor levels when sub-sampled down to two, it would have been infeasible to account for every possible combination. Instead, it was decided to calculate the effect sizes in this manner using five different sub-sample sizes $(10^1, 10^2 ... 10^5)$. The results were then analysed to see if the effect sizes converged. It was found that 10^3 sub-samples were sufficient to converge the effect sizes for all river discharge signatures and projections of snow and ice coverage. Accordingly, this sub-sampling strategy was adopted in this study.

Hydrol. Earth Syst. Sci. Discuss., https://doi.org/10.5194/hess-2018-443
Manuscript under review for journal Hydrol. Earth Syst. Sci.
Discussion started: 5 September 2018

3 Results

3.1 Future climate projections

Projections of temperature for the late 21st century (2076-2100) consistently predict an increase relative to the recent past (1981-2005). The largest increases are predicted for the coldest days of the year during the winter (Figure 5a), spring (Figure 5d) and autumn (Figure 5j) months as shown by the positive skew in the lower sections of the ECDFs. However, these changes are also typically associated with the greatest projection uncertainty. The future climate ensemble projects mean near surface air temperature to rise by between 0.8 and 5.0 ^{o}C by the late 21st century relative to the recent past with an ensemble mean projection of +2.7 ^{o}C.

Projected changes in incident solar radiation span positive and negative values, but the median projections are consistently negative indicating reductions in incident solar radiation are most likely. Uncertainty in the magnitude of change is highest during the spring and summer months (Figures 5e and h) when incident solar radiation peaks. By late 21st century, mean incident solar radiation is projected to change by between -18.5 to +13.0% with an ensemble mean projection of -6.3%.

Projected changes in total precipitation are negligible for the four lowest 10% sections of the precipitation ECDFs, but significant for the two highest sections. In the winter (Figure 5c) and autumn (Figure 5l) months, absolute changes exceed 40 mm d^{-1}. The sign of change is uncertain apart from autumn where median projections are consistently positive for the upper sections of the ECDF. The magnitude of change is also uncertain and by the late 21st century annual precipitation will change by anywhere between -42.8 to +45.5% relative to the recent past with an ensmeble mean projection of +1.2%.

Figure 6 shows the correlation matrix calculated between seasonal average climate variables for late 21st century. For all climate variables, between-season changes (scores within green borders in Fig. 6) are positively correlated indicating that an increase in summer temperature typically corresponds with an increase in winter temperature for example. Temperature has the greatest between-season correlation while precipitation is the least well correlated. Within-season, between-variable correlation scores (within purple border in Fig. 6) show that precipitation and incident solar radiation are negatively correlated and that the correlation between precipitation and temperature depends on the time of year. For the cooler winter, spring and autumn months, temperature and precipitation are positively correlated, but there is a weak negative correlation for the summer months. Temperature and incident solar radiation are negatively correlated, most strongly for the cooler winter, spring and autumn months.

3.2 Future evolution of snow and ice coverage

The ensemble mean projection of annual snow coverage (yellow line in Fig. 7a) indicates that it will decrease from 12.2 km^2 in 2016 to 7.6 km^2 in 2100 (38% reduction). The 95% projection confidence interval indicates that by 2100 the watershed could be almost entirely free of snow (2.9 km^2 remaining) or could have a coverage equivalent to present levels (12.5 km^2).

There is high confidence ($\geq$ 95%) that snow coverage will reduce relative to 2000 levels throughout the 21st century (solid red line line Fig. 7a). Equally high levels of projection confidence apply to projected reductions in snow coverage beyond 2050 relative to 2016 (dashed red line).

Hydrol. Earth Syst. Sci. Discuss., https://doi.org/10.5194/hess-2018-443
Manuscript under review for journal Hydrol. Earth Syst. Sci.
Discussion started: 5 September 2018

Hydrology and Earth System Sciences
Discussions

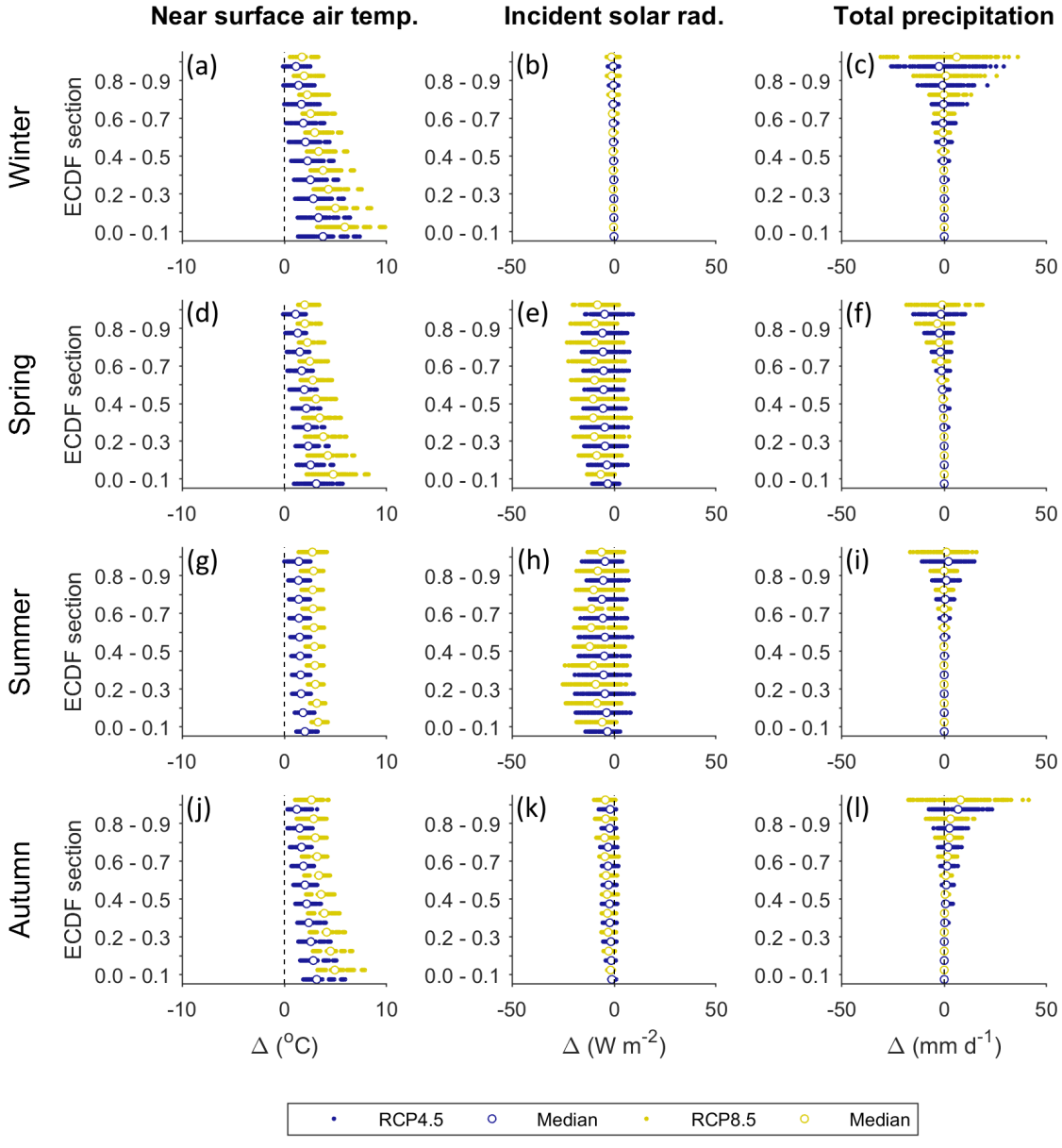

Figure 5. Seasonal average projected changes in ECDFs for near surface air temperature (a,d,g,j), incident solar radiation (b,e,h,k) and total precipitation (c,f,i,l) for the late 21st century (2076-2100) relative to the recent past (1981-2005). Changes are plotted for each 10% section of the ECDFs. For each section, blue and yellow dots represent each of the 140 downscaled future climate time-series for the RCP4.5 and RCP8.5 ES respectively (280 in total). Winter = Dec, Jan, Feb; Spring = Mar, Apr, May; Summer = Jun, Jul, Aug; Autumn = Sep, Oct, Nov.

Hydrol. Earth Syst. Sci. Discuss., https://doi.org/10.5194/hess-2018-443
Manuscript under review for journal Hydrol. Earth Syst. Sci.
Discussion started: 5 September 2018

Hydrology and Earth System Sciences
Discussions

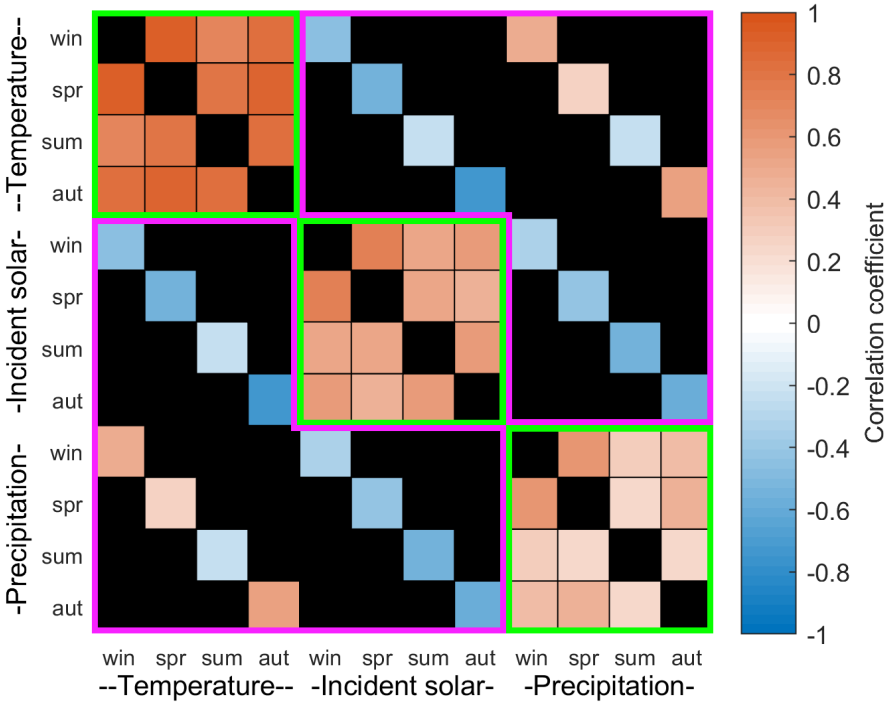

Figure 6. Correlation matrix between seasonal average climate variables calculated for late 21st Century (2076-2100) using the 280 down-scaled future climate time-series. Within-variable, between-season correlation scores are contained within the green borders and within-season, between-variable correlation scores are contained within the purple borders. Those regions of the correlation matrix that do not cover these two groups are shaded in black.

The ensemble mean projection of ice coverage (Figure 7b) predicts a 47% reduction relative to 2016 by 2100. There is high confidence (≥95%) that ice coverage will be less than 2000 and 2016 levels through the remainder of the 21st century, but the magnitude of change is uncertain. By 2100, the 95% confidence interval spans 2.3 km^2 to 11.3 km^2 coverage (12-82% reduction relative to 2016).

The simulations that projected the mean and minimum ice coverage by 2100 both project a sustained retreat of the glacier between 2000 and 2100 (Figure 8). The minimum ice coverage simulation projects that the watershed will be almost entirely ice free by the end of the century. In contrast, the maximum ice coverage simulation projects two periods of glacier advance between 2010 and 2030 and between 2060 and 2100. By the end of the century, this simulation projects ice coverage will be similar to that in 2000.

Figures 9a, b and c show the climate projection time-series that produced the minimum (dotted lines) and maximum (dashed lines) snow (blue lines) and ice (red lines) coverage by 2100. The minimum coverage simulations were forced with some of the highest temperature time-series while the maximum coverage simulations were forced with some of the lowest. The

Hydrol. Earth Syst. Sci. Discuss., https://doi.org/10.5194/hess-2018-443
Manuscript under review for journal Hydrol. Earth Syst. Sci.
Discussion started: 5 September 2018

Hydrology and Earth System Sciences
Discussions

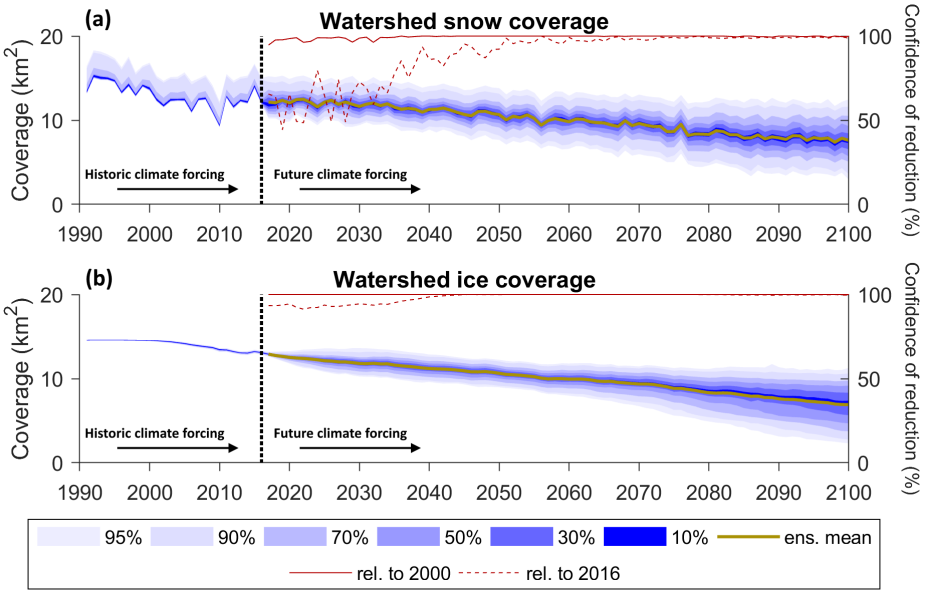

Figure 7. Projected annual watershed snow coverage (a) and ice coverage (b) including the projection confidence intervals (blue bands) and ensemble mean projections (yellow lines). Also shown are projection confidence levels for a reduction in coverage relative to 2000 and 2016 (red lines).

maximum coverage simulations show higher than average incident solar radiation inputs (Figure 9b) and lower precipitation volumes than the minimum coverage simulations. Indeed, correlation scores calculated between seasonal average climate variables and the simulated snow and ice coverage by 2100 (Figure 9d) show that there is a strong negative correlation between mean temperature and projected snow and ice coverage and a weaker positive correlation between snow and ice coverage and incident solar radiation. An even weaker negative correlation exists between autumn and winter precipitation and snow and ice coverage.

3.3 Sources of uncertainty in snow and ice coverage projections

The effect size of the main, interaction and error terms calculated using ANOVA for projected changes in decadal snow and ice coverage are shown in Fig. 10. Note, ROR effects are not included here as this model chain component has no influence on cryospheric processes in the GHM. The effect size of each ANOVA term changes through the decades and also varies between snow and ice coverage. Throughout the 21st century, TIM uncertainty contributes <3% to the total projection uncertainty of snow coverage. For projections of ice coverage, η^2_{TIM}>0.12 for the first half of the 21st century, but then gradually falls to 0.06 by the 2090s. η^2_{DS} and η^2_I never exceed 0.2 for snow and ice coverage and as with η^2_{TIM}, they gradually reduce through the 21st century. GCM-RCM uncertainty is the largest contributor to projection uncertainty in the 2020s with effect sizes of

Hydrol. Earth Syst. Sci. Discuss., https://doi.org/10.5194/hess-2018-443
Manuscript under review for journal Hydrol. Earth Syst. Sci.
Discussion started: 5 September 2018

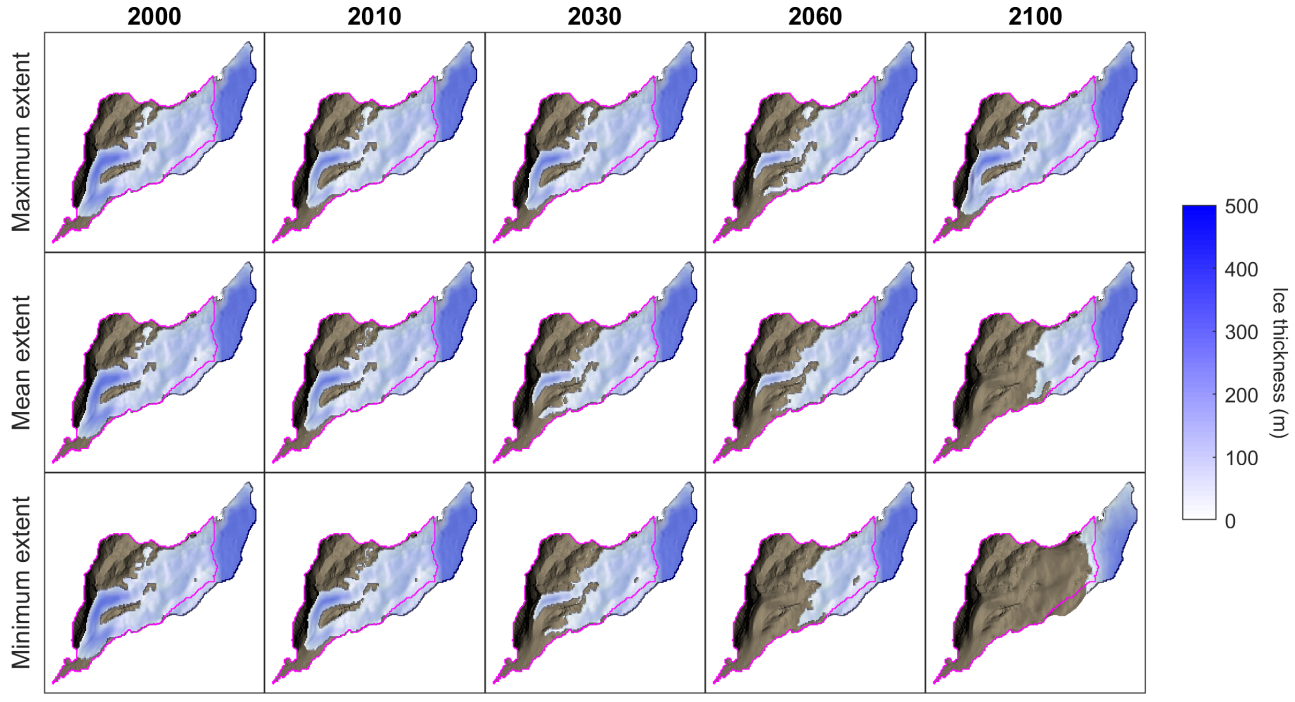

Figure 8. Simulated ice thickness between 2000 and 2100 based on simulations that projected the maximum, mean and minimum ice coverage by 2100. Watershed outline shown in magenta.

0.45 and 0.51 for snow and ice coverage respectively. However, for the mid and latter half of the 21st century ES uncertainty dominates, contributing 71% and 72% of the total projection uncertainty of snow and ice coverage by the 2090s.

3.4 Future evolution of primary runoff components

As an initial indication of the potential for downstream river flow regime change, Fig. 11 shows the decadal evolution of changes in the four primary runoff components relative to the 1990s including the ensemble mean projections of change (yellow dots) and their respective projection confidence intervals (blue bands). The ensemble mean indicates rainfall will increase relative to the 1990s for all months except August, but particularly during the autumn (SON) and winter (DJF) months (Figure 11a). The confidence in the sign of change for these months is $\geq$85% by the 2090s. A comparison of the 1990s and 2090s monthly ensemble means (black lines) indicates that rainfall will more than double for majority of the autumn and winter months.

For snowmelt, the greatest changes are projected to occur in the summer months (JJA) where there is $\geq$85% confidence that melt will reduce relative to the 1990s throughout the 21st century (Figure 11b). The ensemble mean projects that summer melt will reduce by 40-50% by the 2090s and that the annual melt will decrease by 28%. A similar pattern of change is projected for

Hydrol. Earth Syst. Sci. Discuss., https://doi.org/10.5194/hess-2018-443
Manuscript under review for journal Hydrol. Earth Syst. Sci.
Discussion started: 5 September 2018

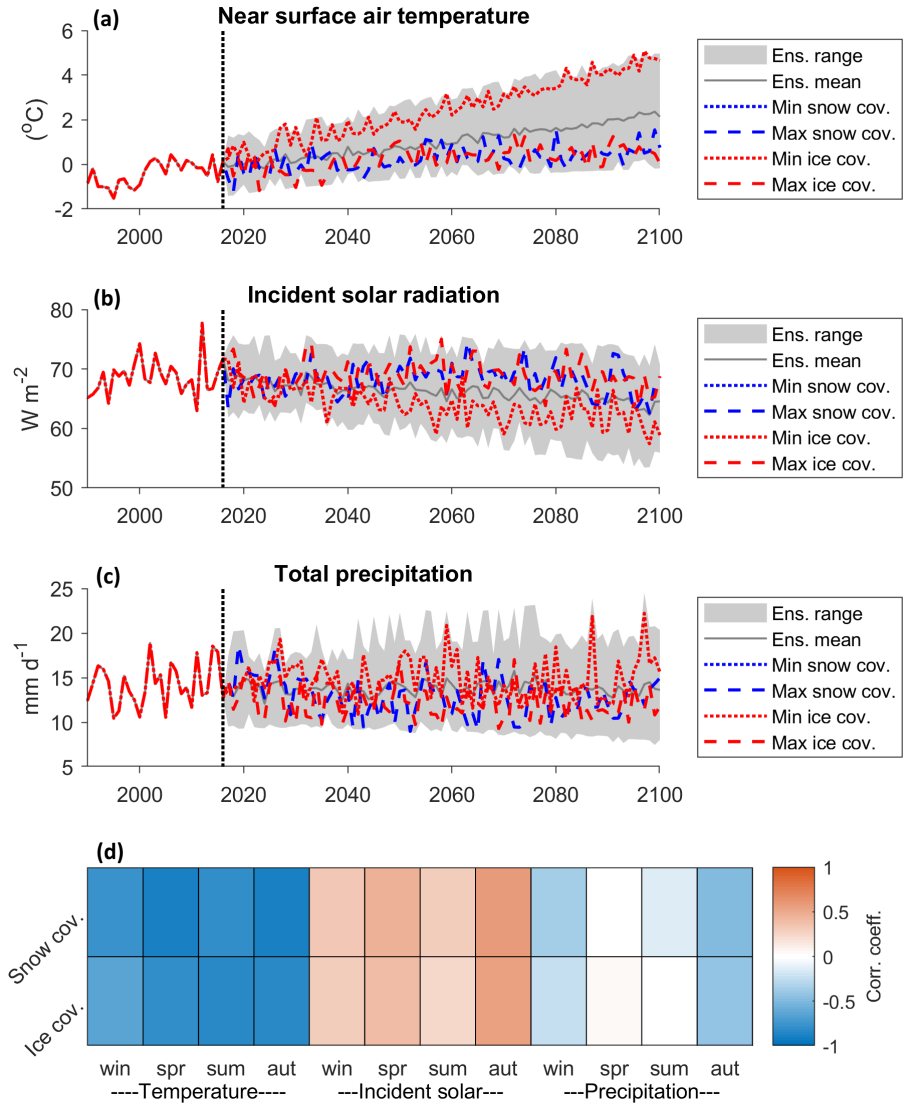

Figure 9. Relationship between driving climate data and projected snow and ice coverage including annual mean downscaled climate time-series of temperature (a), incident solar radiation (b) and total precipitation (c) with time-series that produced the minimum (dotted lines) and maximum (dashed lines) snow and ice coverage by the end of 2100. Also included are correlation scores calculated between seasonal average climate variables over the entire future period (2017-2100) and simulated snow and ice coverage by the end of 2100 (d).

Hydrol. Earth Syst. Sci. Discuss., https://doi.org/10.5194/hess-2018-443
Manuscript under review for journal Hydrol. Earth Syst. Sci.
Discussion started: 5 September 2018

Hydrology and Earth System Sciences
Discussions

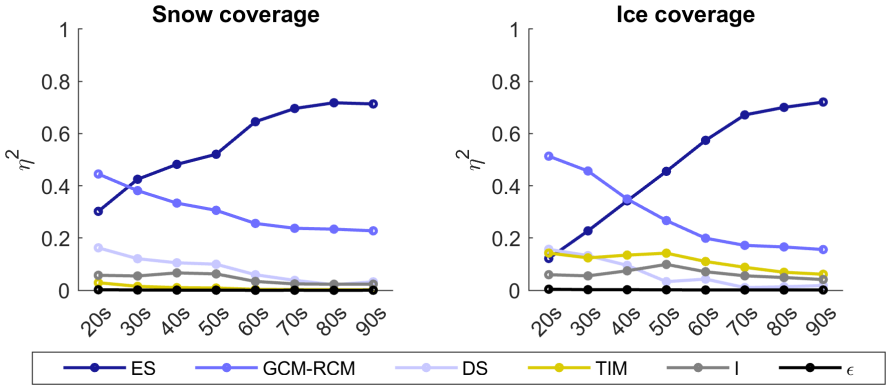

Figure 10. Effect size (η^2) of main effects, interactions and remaining error calculated using ANOVA on projected decadal changes in snow and ice coverage. Note, the ROR main effect is not included here as it does not influence cryospheric processes in the GHM.

ice melt (Figure 11c) with the largest proportional reduction in melt projected for June (61%) by the 2090s. A small increase in winter ice melt is projected for the early and mid 21st century relative to the 1990s, but by the 2090s, winter melt is projected to reduce to near-1990s levels on average with an overall decrease in annual melt of 45%.

Projections consistently predict an increase in evapotranspiration throughout the year (Figure 11d) with the largest increases projected for the end of the 21st century. However, the volume of evapotranspiration remains a small component of the overall water balance throughout the 21st century.

3.5 Future evolution of river flow regime

Figure 12 shows the projected decadal changes in river discharge signatures relative to the 1990s (except peak water for which the raw projections are shown). The 95% projection bounds of the peak water (PW) signature indicate that it may have occurred in 2002 or could occur as late as 2089. Indeed, the sign of change of the mean annual flow signature ($\bar{Q}$) relative to the 1990s is also uncertain as shown by the confidence intervals which are approximately evenly distributed between positive and negative changes. By the end of the 21st century though, annual flow is projected to remain close to 1990s on average (ensemble mean projects 8% decrease for 2090s). In contrast, there is much higher confidence ($\geq$75%) that inter-annual flow range (R_{ANN}) will be higher throughout the 21st century relative to the 1990s. The ensemble mean projects a 0.6 m^3 s^{-1} (60%) increase in R_{ANN} by the 2090s.

Seasonally, monthly winter (DJF) flows are projected to increase with high confidence (>85%) while >90% of the ensemble project a decrease in summer (JJA) flows by the 2090s. The absolute change in mean monthly flows is larger for summer flows on average, but proportionally, the winter flows are projected to change most, particularly in February where the ensemble mean projects an increase of 212%. The combined effect of increased winter flows and decreased summer flows results in decreased intra-annual flow variability. More than 95% of the ensemble project a decrease in R_{mnth} relative to the 1990s and the ensemble mean projects a decade-on-decade reduction in R_{mnth} with time.

Hydrol. Earth Syst. Sci. Discuss., https://doi.org/10.5194/hess-2018-443
Manuscript under review for journal Hydrol. Earth Syst. Sci.
Discussion started: 5 September 2018

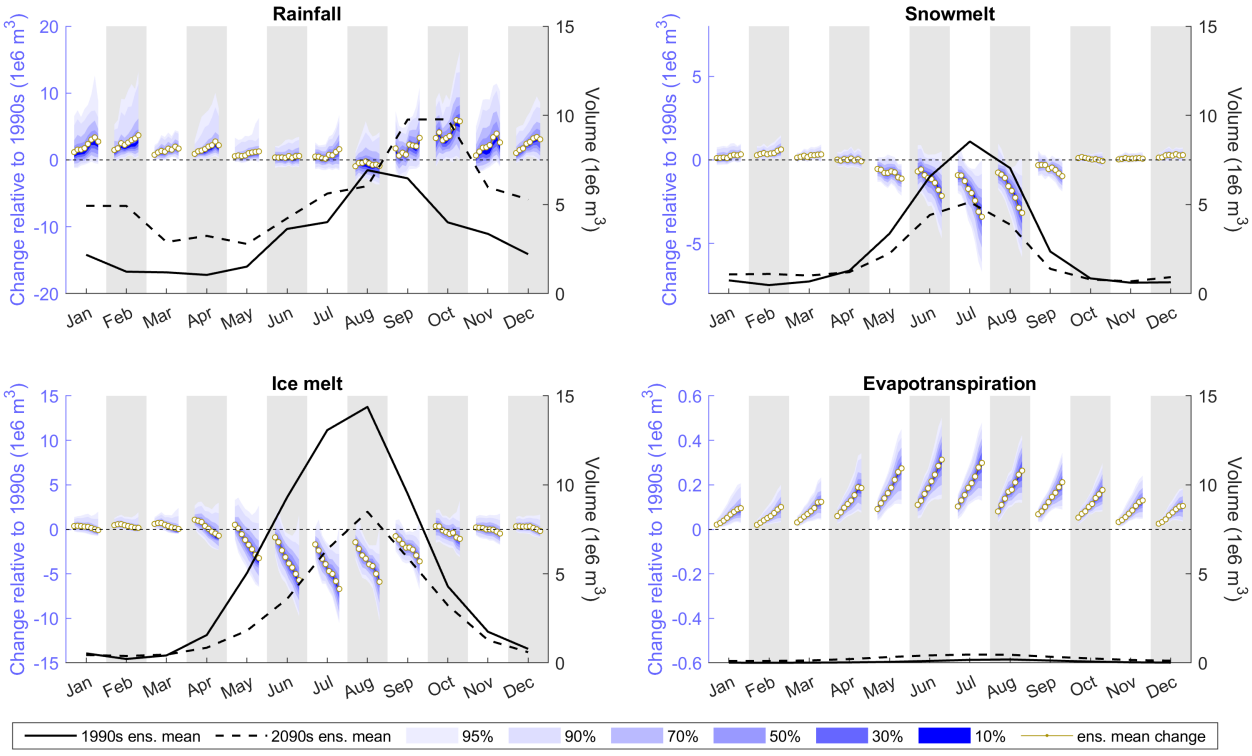

Figure 11. Projections of monthly mean runoff components including rainfall (a), snowmelt (b), ice melt (c) and evapotranspiration (d). Each plot includes projected decadal changes (2020s to 2090s) relative to the 1990s with projection confidence intervals (blue bands) and ensemble mean projections (yellow dotted lines) and ensemble mean monthly runoff volume averaged over the 1990s (black solid line) and 2090s (black dash line). Note, the monthly runoff volumes are plotted on the same scale for all runoff components to allow for cross-comparison.

Of those signatures with units $m^3\ s^{-1}$, the high flow Q_{01} signature shows the largest ensemble mean change of just under 5 $m^3\ s^{-1}$ by the 2090s, an increase of 28% relative to the 1990s. There is high confidence (≥85%) that Q_{01} will increase relative to the 1990s but the magnitude of change is uncertain (-2.5 to 15.7 $m^3\ s^{-1}$). The sign of change for Q_{05} is less certain and by the 2090s the 95% confidence bounds indicate it could increase by 4.4 $m^3\ s^{-1}$ or decrease by 3.3 $m^3\ s^{-1}$. Projections of changes to high flow variability (σ_{05-01}) are consistently positive with an average increase of 1.4 $m^3\ s^{-1}$ (91%) by the 2090s.

For moderate flows, the ensemble mean projects a small increase in Q_{50} of 0.6 $m^3\ s^{-1}$ for the 2020s which then gradually trends towards a small, negative change by the 2090s. The sign of change is uncertain, particularly towards end of century. However, moderate flow variability (σ_{52-48}) is consistently projected to reduce, albeit by only 0.05 $m^3\ s^{-1}$ (31%), by the 2090s.

For the slow-release low flow signatures, projections are consistently positive throughout the 21st century indicating an increase in the magnitude of low flow events (or equivalently a reduction in the frequency of these flow events) and variability of low flows. The absolute change in the ensemble mean never exceeds 0.2 $m^3\ s^{-1}$ for these signatures, although proportionally, they show the largest degree of change, particularly for Q_{99} where the proportional change exceeds 6000%.

Hydrol. Earth Syst. Sci. Discuss., https://doi.org/10.5194/hess-2018-443
Manuscript under review for journal Hydrol. Earth Syst. Sci.
Discussion started: 5 September 2018

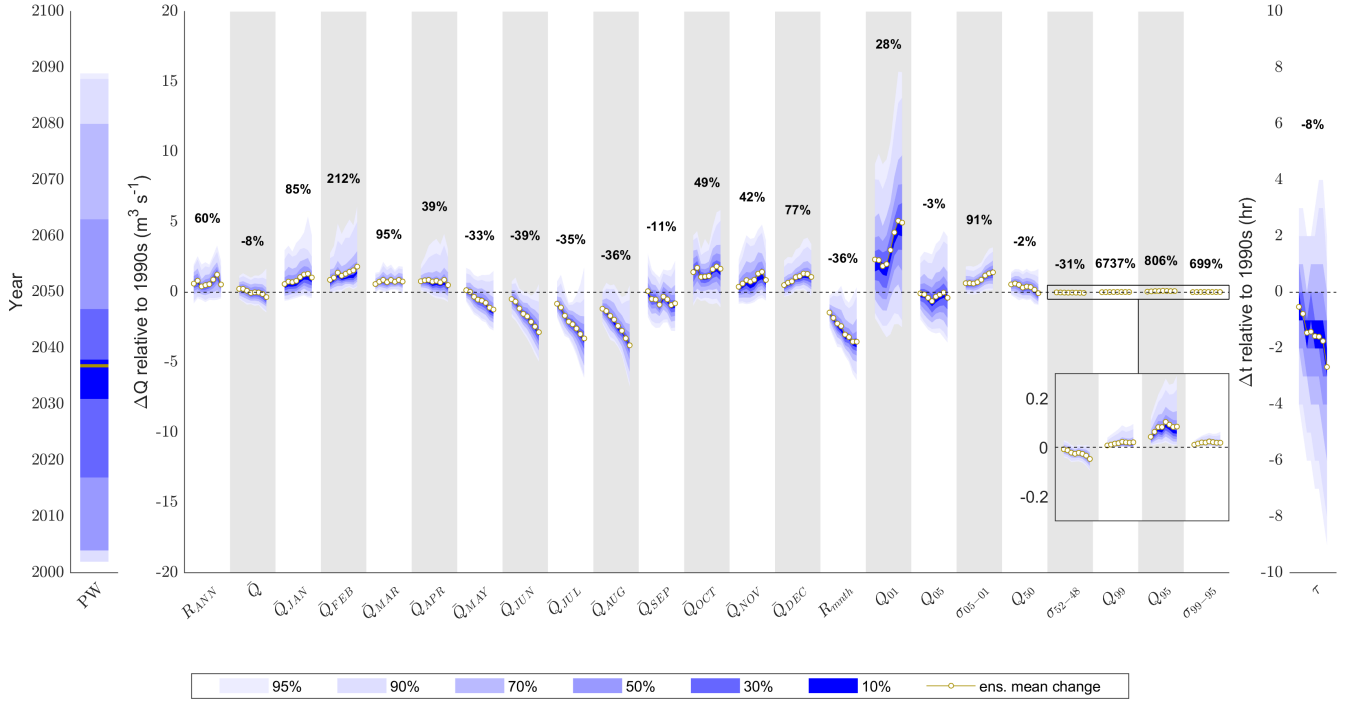

Figure 12. Projected decadal changes in river discharge signatures for 2020s to 2090s relative to 1990s including projection confidence intervals (blue bands) and ensemble mean projections (yellow dotted lines). Also shown are 2090s ensemble mean change expressed as a percentage of simulated signatures for 1990s. Note the peak water (PW) signature is not expressed as decadal chnages, but as the overall raw projections.

Finally, the response time to runoff (τ) is projected to decrease by the 2090s ($\geq$75% confidence) indicating the catchment will likely become more flashy. The magnitude of change is small where the ensemble mean projects a small reduction in τ of 2.6 hours.

3.6 Sources of uncertainty in river flow regime projections

Figure 13 shows the ANOVA effect sizes averaged across the future decades (2020s to 2090s) for each river discharge signature. The error term (η^2_ϵ) never exceeds 0.09 and for 21 of the 25 signatures is < 0.03 indicating that the main effects and first order interaction terms explain the majority of projection uncertainty. Of these, ES uncertainty contributes 7-29% of the total projection uncertainty across the signatures. The five signatures with the highest η^2_{ES} are the mean monthly flows between May and August, and October (Table 2) for which the effect sizes are at least 0.25. GCM-RCM uncertainty is the largest contributor to total projection uncertainty for 19 of the 25 river discharge signatures. $\eta^2_{GCM-RCM}$ exceeds 0.4 for the five most sensitive signatures to GCM-RCM uncertainty (Table 2) which include mean annual flow ($\bar{Q}$), mean monthly flows for

Hydrol. Earth Syst. Sci. Discuss., https://doi.org/10.5194/hess-2018-443
Manuscript under review for journal Hydrol. Earth Syst. Sci.
Discussion started: 5 September 2018

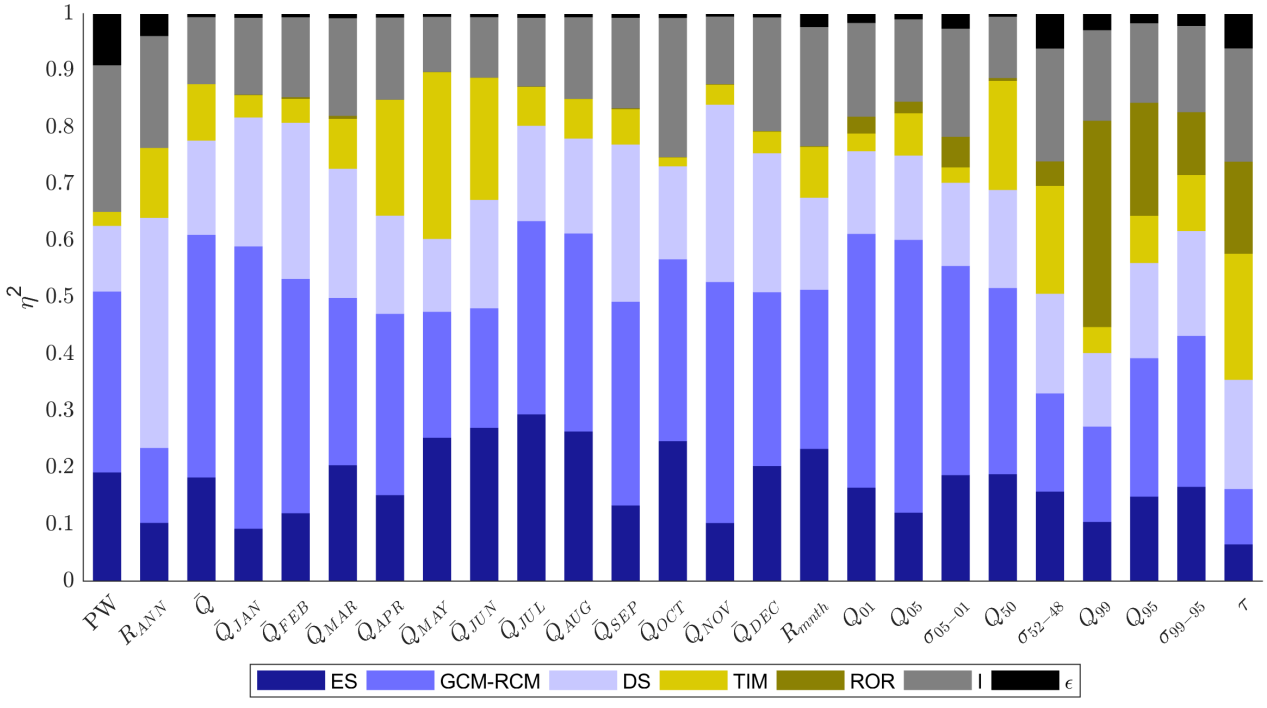

Figure 13. Effect size (η^2) of all main effects, interactions and remaining error on projected decadal changes in the 25 river discharge signatures averaged across all decades affected by future climate change (2020s to 2090s).

November and January and two of the quick-release high flow signatures (Q_{01} and Q_{05}). Uncertainty stemming from the DS parameterisation contributes 12-41% of the total projection uncertainty across the signatures. DS is also the largest contributor to projection uncertainty for the inter-annual flow range (R_{ANN}) projections. Indeed, it exceeds the combined effect of all the remaining main effects. Autumn and winter monthly mean flows for September, November, December and February make up the remainder of the top five signatures most effected by DS uncertainty. TIM uncertainty contributes $\geq$20% of the mean monthly flow projection uncertainty between April and June at the beginning of the melt season. It is also the largest contributor to uncertainty of projections of response time to runoff (τ) where $\eta^2_{TIM} = 0.22$. Uncertainty stemming from the ROR structure-parameterisation has a negligible influence on the decadal signatures (PW and R_{ANN}) or those signature characterising annual and monthly mean flows. It does, however, show to be important for projections of low flow magnitude (Q_{99} and Q_{95}, $\eta^2_{ROR} =$ 0.36 and 0.20 respectively) and variability ($\sigma_{99\text{-}95}$, $\eta^2_{ROR} = 0.11$). In fact, for Q_{99}, ROR is the single largest contributor to total projection uncertainty. 16% of the τ projection uncertainty also stems from the ROR structure-parameterisation. Unlike ice and snow coverage, interactions between model components significantly contribute the total projection uncertainty across the signatures where η^2_I ranges between 0.1 and 0.26. There is no clear pattern in the relative effect size of the interaction term across the signatures, but the five signatures with the largest η^2_I include PW, $\bar{Q}_{OCT}$, R_{mnth}, $\bar{Q}_{DEC}$ and τ. Figure 14 shows the

Hydrol. Earth Syst. Sci. Discuss., https://doi.org/10.5194/hess-2018-443
Manuscript under review for journal Hydrol. Earth Syst. Sci.
Discussion started: 5 September 2018

Hydrology and Earth System Sciences
Discussions

Table 2. Top five river discharge signatures ranked according to the average effect size for each of the main effects, interactions and remaining error on projected decadal changes. Effect sizes are included in brackets.

Rank	ES (η^2_{ES})	GCM-RCM ($\eta^2_{GCM-RCM}$)	DS (η^2_{DS})	TIM (η^2_{TIM})	ROR (η^2_{ROR})	I (η^2_I)	ϵ (η^2_ϵ)
1	$\bar{Q}_{JUL}$ (0.29)	$\bar{Q}_{JAN}$ (0.50)	R_{ANN} (0.41)	$\bar{Q}_{MAY}$ (0.29)	Q_{99} (0.36)	PW (0.26)	PW (0.09)
2	$\bar{Q}_{JUN}$ (0.27)	Q_{05} (0.48)	$\bar{Q}_{NOV}$ (0.31)	τ (0.22)	Q_{95} (0.20)	$\bar{Q}_{OCT}$ (0.25)	$\sigma_{52\text{-}48}$ (0.06)
3	$\bar{Q}_{AUG}$ (0.26)	Q_{01} (0.45)	$\bar{Q}_{SEP}$ (0.28)	$\bar{Q}_{JUN}$ (0.22)	τ (0.16)	R_{mnth} (0.21)	τ (0.06)
4	$\bar{Q}_{MAY}$ (0.25)	$\bar{Q}$ (0.43)	$\bar{Q}_{FEB}$ (0.28)	$\bar{Q}_{APR}$ (0.20)	$\sigma_{99\text{-}95}$ (0.11)	$\bar{Q}_{DEC}$ (0.20)	R_{ANN} (0.04)
5	$\bar{Q}_{OCT}$ (0.25)	$\bar{Q}_{NOV}$ (0.42)	$\bar{Q}_{DEC}$ (0.25)	Q_{50} (0.19)	$\sigma_{05\text{-}01}$ (0.05)	τ (0.20)	Q_{99} (0.03)

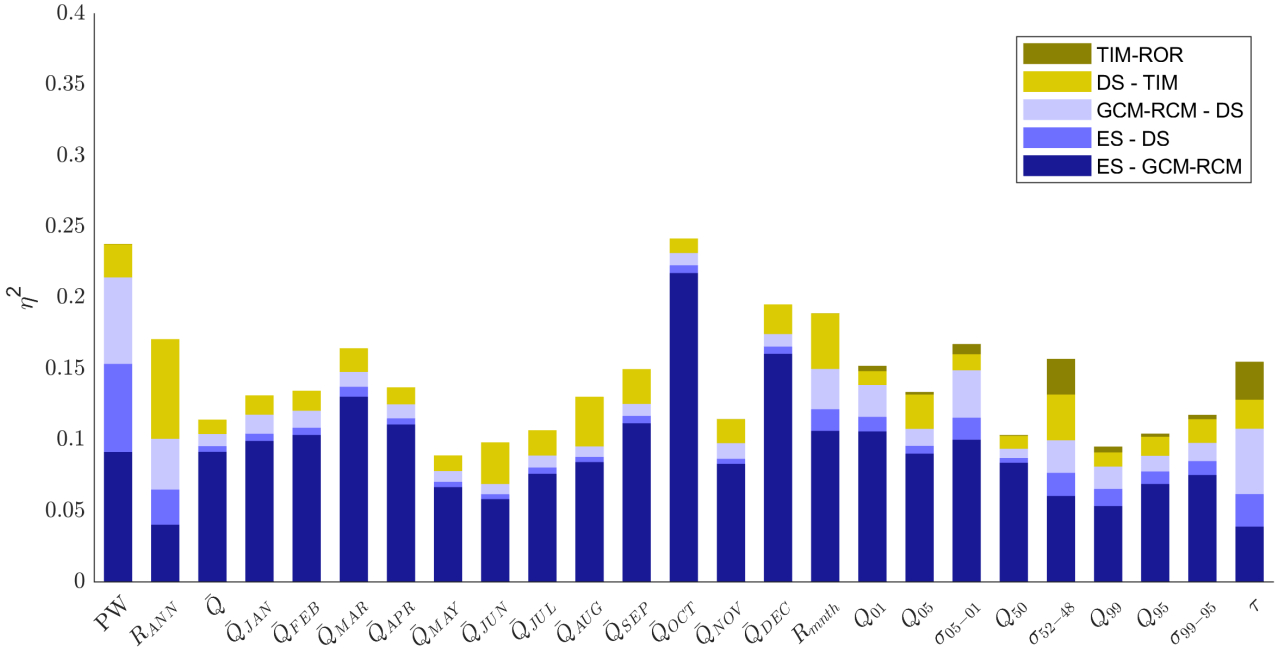

Figure 14. Effect size (η^2) of the five most significant interactions on projected decadal changes in the 25 river discharge signatures averaged across all decades affected by future climate change (2020s to 2090s).

decomposition of the five interaction terms with the largest effect sizes on average. Generally, it is the interaction between the ES and GCM-RCM model chain components that dominate the contribution to projection uncertainty. However, interactions between the climate model chain components and the GHM (e.g. DS-TIM) may also contribute to the projection uncertainty. For R_{ANN}, DS-TIM interaction contributes 5% of total projection uncertainty. Furthermore interactions between the TIM and ROR in the GHM contribute some (albeit small) amounts to the total projection uncertainty.

Hydrol. Earth Syst. Sci. Discuss., https://doi.org/10.5194/hess-2018-443
Manuscript under review for journal Hydrol. Earth Syst. Sci.
Discussion started: 5 September 2018

4 Discussion

4.1 Future evolution of river flow regime

There is high confidence that near-surface air temperature will increase by the late 21st century (2076-2100) relative to conditions in the recent past (1981-2005). Precipitation and incident solar radiation were projected to slightly increase and decrease respectively on average: a finding that is consistent with other analyses of the EURO-CORDEX projections for northern Europe (Bartók et al., 2017). The primary driver of changes in snow and ice is near-surface air temperature, while precipitation and incident solar radiation are of secondary importance. Because of this, there is high confidence that glacier ice and snow will continue to retreat as near-surface air temperature rises throughout the 21st century which would leave the river basin almost free of snow and ice by 2100 under the warmest climate projections.

The propagation of change from climate and cryosphere to the hydrosphere is clear for the Virkisá river basin and the signature-based analysis revealed that these changes will ultimately impact the magnitude, timing and variability of downstream river flows over a range of timescales. Seasonally, the loss of snow and ice will reduce meltwater inputs in the summer months (-37% by 2090s) where flows are currently highest on average. Additionally, a phase shift of precipitation from snowfall to rainfall combined with enhanced melt during the colder months will increase winter runoff (113% by the 2090s) where monthly flows are currently lowest on average. The consequence of these seasonal shifts in runoff is that intra-annual (monthly) flow variability will reduce (-36% by 2090s). Furthermore, the magnitude of very low flow events (Q_{99}), which typically occur during the winter months, are likely to increase. Equivalently, the frequency of very low flow events, as defined by the 1990s reference Q_{99} flow, will decrease.

On average, the projections indicated that the seasonal redistribution of runoff will have little influence on mean annual flows (-8% by 2090s) as changes in summer and winter flows approximately compensate one-another. However, the loss of a consistent melt input to the river basin and its evolution to a hydrological regime governed by rainfall-runoff processes means inter-annual flow variability (R_{ANN}) will increase (+60% by 2090s). The increase in rainfall inputs, particularly during the storm-prone autumn and winter months, likely explains the projected increased magnitude of very high flow events (Q_{01}) and the intensification of peak flow magnitudes will be further exacerbated by the projected decrease in river flow response time to runoff (τ): an artefact of losing the runoff-regulating ice and snow water stores. Accordingly, the river basin will become more flashy and flood-prone in the future.

Increased flood frequency has major implications to local infrastructure in the vicinity of the Virkisá river basin. In particular, the southern section of the Route 1 highway which passes over the Skeiðarársandur floodplain navigates a large number of glacier-fed rivers including the Virkisá. Due to the unconsolidated nature of the floodplain lithology, the morphology of these rivers can change rapidly, particularly during high flow events (Marren, 2005) and often at considerable expense to the road authority (Björnsson and Pálsson, 2008). Accordingly, the projected increase in frequency and severity of high flow events will likely incur further expenses to maintain this transport link in the future.

Beyond local implications, one should be cautious in extrapolating the findings from this study to other glaciated catchments in Iceland or beyond as the sign and magnitude of river flow regime response is likely to be dependent on catchment

characteristics such as climate, glacier hypsometry and geology. Even so, it can be concluded from this study that the timing, magnitude and variability of glacier-fed river flows over a range of timescales are sensitive to climate change. For Iceland, these changes could impact glacier-fed hydroelectric dams: a primary source of electricity for the country. Increased frequency and magnitude of high flow events could render current dams unsafe if their designed flood capacity can no longer meet regulation requirements (Thorsteinsson and Björnsson, 2012). The redistribution and 'levelling out' of seasonal flows, however, could actually have a beneficial effects on the running costs and capacity to produce electricity from such projects (Jóhannesson et al., 2007).

Outside of Iceland, changes to low flow magnitudes are undoubtedly important for regions that rely on river water for drinking and irrigation. In this study a small absolute increase in low flow magnitude was projected indicating climate change and deglaciation could help to limit periods of water scarcity. However, in more arid regions, where rainfall cannot compensate reductions in melt, one might expect to see the opposite effect (Ragettli et al., 2016). One might also expect to see much greater changes in the river flow response time to runoff as snow and ice retreat in other river basins. For the Virkisá river basin, a relatively small reduction in response time (τ) was projected on average by the end of the 21st century. This, perhaps, should not be surprising given the small size of the river basin and the fact that previous investigations have shown that Virkisjökull has a well developed conduit drainage system that routes runoff efficiently year-round (Phillips et al., 2014; Flett et al., 2017). For larger river basins with more expansive cryopsheric water stores, changes in the response time to runoff could be much greater, substantially increasing the risk of pluvial flooding. It is therefore vital that signature-based evaluations like the one undertaken in this study are applied to other glaciated river basins in the future so that regional variations in river flow regime change can be evaluated.

4.2 Uncertainties in projections of river flow regime

Projections of the sign of change relative to the 1990s reference period were well constrained for the majority of river discharge signatures, particularly towards the end of the 21st century. Even so, there was considerable spread in the projected magnitude of these changes due to uncertainties in the driving climate data (ES,GCM-RCM,DS) and representation of glacio-hydrological processes (TIM,ROR) in the model chain. Generally, sources of climate uncertainty had a larger influence on the spread of projections than those stemming from the GHM, but the relative importance of the five different model chain components was dependent on which signature of river discharge was being evaluated. Uncertainty in future snow and ice coverage primarily stemmed from the ES, and consequently the ES was also the dominant source of uncertainty in projections of mean monthly flows during the melt season. In contrast, the spread of projected mean monthly winter flows stemmed mainly from GCM-RCM uncertainty, presumably because of the considerable spread in projections of the highest precipitation magnitudes between the different GCM-RCMs. Indeed, this would also explain why uncertainties in the projections of signatures representing quick-release high flows were most influenced by the choice of GCM-RCM.

For projections of the inter-annual flow range, the DS procedure was the largest contributor to projection uncertainty, which should be expected given that the perturbation of this procedure accounted for uncertainty in the random year-by-year sampling of the historic climate data. Uncertainty in the TIM structure-parameterisation was the dominant contributor to the spread in

projections of moderate monthly flows during the transition from the cold to melt season which corroborates with the model comparison study of Mackay et al. (2018) who found that the structural representation of melt was important for controlling the initiation of the melt season due to the contrasting sensitivity of the models to temperature and incident solar radiation. Mackay et al. (2018) also concluded that signatures derived from the flow duration curve as well as those representing flashiness were most sensitive to the configuration of the ROR component of the GHM. Indeed, here it was found that uncertainty in the ROR structure-parameterisation significantly contributed to the total projection uncertainty of slow-release low flow signatures as well as the response time (flashiness) of the catchment to runoff.

These findings have two key implications for the design of model experiments that seek to project changes in river flow regime in glaciated river basins. Firstly, studies should seek to represent uncertainties stemming from model chain components that control future climate and glacio-hydrological behaviour, the second of which has been widely neglected. The need for this is compounded by the fact that interactions between model chain components exceeded individual main effects for some river discharge signatures. Accordingly, an ensemble that includes perturbations of multiple components of the model chain simultaneously will provide the most rigorous quantification of projection uncertainty.

Secondly, if one is interested in projecting specific characteristics of river flow regime, the experiment may be designed in such a way as to prioritise quantification of the dominant sources of projection uncertainty. For example, the results from this study indicate that for evaluating changes in monthly melt season runoff only, it may be beneficial to ignore ROR uncertainty and focus time and computational resources on quantifying uncertainties stemming from the remaining model components. In this respect, the time frame of the projections should also be considered, given the apparent change in effect sizes with time demonstrated for projections of snow and ice coverage. Similar time-variance in effect sizes were also found for the river flow signatures (see Appendix C).

5 Conclusions

21st century climate change is projected to alter the magnitude, timing and variability of river flows over decadal to sub-daily timescales in the Virkisá river basin. Relative to the 1990s reference period, there was high confidence in the sign of change for the majority of the 25 river discharge signatures over the 21st century. The magnitude of change, however, was more uncertain. The application of ANOVA demonstrated that the climate model chain components (ES,GCM-RCM,DS) were the main sources of this uncertainty. However, uncertainty relating to glacio-hydrological process representation in the model chain (TIM,ROR) were the dominant source of projection uncertainty for some river discharge signatures. Furthermore, interactions between model chain components can exceed individual main effects. Based on these findings, we make several recommendations for future studies that aim to assess climate change impact on glacier-fed river flows:

1. Studies should seek to evaluate multiple characteristics of river flow regime change (magnitude, timing and variability) over different timescales where possible so that a more thorough understanding of potential environmental and socio-economic impacts can be deduced from projections. Signatures of river discharge provide the ideal tool to evaluate these changes quantitatively. Changes in the magnitude of river flows over decadal to seasonal timescales are already known to

Hydrol. Earth Syst. Sci. Discuss., https://doi.org/10.5194/hess-2018-443
Manuscript under review for journal Hydrol. Earth Syst. Sci.
Discussion started: 5 September 2018

Hydrology and Earth System Sciences
Discussions

Table A1. Summary of 12 ice melt and snow coverage signatures used to calibrate the GHM with their limits of acceptability.

Attribute	Signature	Limits of acceptability
Seasonal ice melt on tongue	2013 Summer ice melt	5.22 – 6.44 m we
	2012-2013 Winter ice melt	0.64 – 0.78 m we
Long term glacier volume change	Change in ice volume (1988-2011)	-0.36 – -0.28 km^3
Snow coverage in lower catchment	Mean snow coverage in spring	0.32 – 0.45
	Mean snow coverage in early summer	0.02 – 0.08
	Mean snow coverage in late summer	0.00 – 0.03
Snow coverage in mid catchment	Mean snow coverage in spring	0.70 – 0.80
	Mean snow coverage in early summer	0.17 – 0.27
	Mean snow coverage in late summer	0.00 – 0.04
Snow coverage in upper catchment	Mean snow coverage in spring	0.81 – 0.90
	Mean snow coverage in early summer	0.51 – 0.64
	Mean snow coverage in late summer	0.02 – 0.09

be highly site-specific and therefore we should expect that other signatures of regime change will also show considerable inter-catchment variation.

2. Studies should account for uncertainties stemming from both the climate projections and glacio-hydrological process representations so that more robust projections of river flow regime change are produced. The latter has largely been neglected in studies to date.

3. Careful consideration of which model chain components are the dominant sources of projection uncertainty (through the use of methods such as ANOVA) would help to prioritise resources (e.g. computational) to further enhance projection robustness. The results from this study indicate that such decisions will depend on the signatures of river flow regime change that one is interested in projecting.

Appendix A: Ice melt and snow coverage signatures used for model calibration

12 signatures of ice melt and snow coverage which were previously derived by Mackay et al. (2018) were used for model calibration and are shown in Table A1. These signatures include: i) measurements of winter and summer ice melt in the main ablation zone between 2012 and 2014 which were derived from ablation stake data; ii) an estimate of long-term glacier volume change calculated using two DEMs of the ice for 1988 and 2011; and iii) estimates of the average seasonal snow coverage (spring, early summer, late summer) in the lower, mid and upper sections of the study basin calculated from the remotely-sensed MOD10A1 MODIS product (Riggs and Hall, 2015).

Hydrol. Earth Syst. Sci. Discuss., https://doi.org/10.5194/hess-2018-443
Manuscript under review for journal Hydrol. Earth Syst. Sci.
Discussion started: 5 September 2018

Hydrology and Earth System Sciences
Discussions

Table B1. Calibration parameters for the melt and runoff-routing model structures.

Structure	Parameter	Description	Calibration range	Units
TIM_1	a_{ice}	Temperature factor for bare ice	2.0e-4 - 7.0e-4	m we $^oC^{-1}$ hr^{-1}
	$a_{snow/firn}$	Temperature factor for snow/firn	4.0e-7 - 2.0e-4	m we $^oC^{-1}$ hr^{-1}
TIM_2	a_{ice}	Temperature factor for bare ice	2.0e-4 - 7.0e-4	m we $^oC^{-1}$ hr^{-1}
	$a_{snow/firn}$	Temperature factor for snow/firn	4.0e-7 - 2.0e-4	m we $^oC^{-1}$ hr^{-1}
	b_{ice}	Radiation factor for bare ice	4.0e-7 - 2.0e-6	m^3 we W^{-1} $^oC^{-1}$ hr^{-1}
	$b_{snow/firn}$	Radiation factor for snow/firn	4.0e-8 - 4.0e-7	m^3 we W^{-1} $^oC^{-1}$ hr^{-1}
TIM_3	a_{ice}	Temperature factor for bare ice	1.5e-4 - 3.0e-4	m we $^oC^{-1}$ hr^{-1}
	$a_{snow/firn}$	Temperature factor for snow/firn	6.0e-5 - 2.0e-4	m we $^oC^{-1}$ hr^{-1}
	b_{ice}	Radiation factor for bare ice	1.0e-5 - 8.0e-5	m^3 we W^{-1} hr^{-1}
	$b_{snow/firn}$	Radiation factor for snow/firn	2.0e-7 - 4.0e-6	m^3 we W^{-1} hr^{-1}
	p_2	Dynamic snow albedo parameter for Brock et al. (2000) model	0.01 - 0.4	
ROR_1	k	Mean residence time of reservoir	1 - 30	hr
	n	Number of reservoirs	1 - 5	
ROR_2	$k_{ice/soil}$	Mean residence time of runoff from ice and soil	0.1 - 5	hr
	$k_{snow/firn}$	Mean residence time of runoff from snow and firn	20 - 100	hr
	$n_{ice/soil}$	Number of reservoirs in ice/soil cascade	1 - 5	
	$n_{snow/firn}$	Number of reservoirs in snow/firn cascade	1 - 5	

Appendix B: GHM calibration parameters

Table B1 lists all of the calibration parameters and their pre-defined calibration ranges for the melt and runoff-routing model structures used during the GHM calibration procedure. The three melt model structures include the classic temperature index model (TIM_1), the enhanced temperature-index model proposed by Hock (1999) (TIM_2) and the enhanced temperature-index model proposed by Pellicciotti et al. (2005) (TIM_3). The two runoff-routing model structures include the single linear reservoir cascade (ROR_1) and two linear reservoir cascades in parallel (ROR_2).

Appendix C: Decadal changes in effect size for river discharge signatures

Author contributions. JDM undertook all practical elements of this study including regional climate projection downscaling, GHM calibration, 21st century projections, ANOVA, analysis of results and production of figures. He also led the writing of this manuscript. JE and ARB managed the design, commissioning and operation of the hydro-meteorological monitoring used in this study. All co-authors contributed to formulation and discussion of methods used as well as writing of the manuscript.

Competing interests. The authors declare they have no competing interests.

Hydrol. Earth Syst. Sci. Discuss., https://doi.org/10.5194/hess-2018-443
Manuscript under review for journal Hydrol. Earth Syst. Sci.
Discussion started: 5 September 2018

Hydrology and Earth System Sciences
Discussions

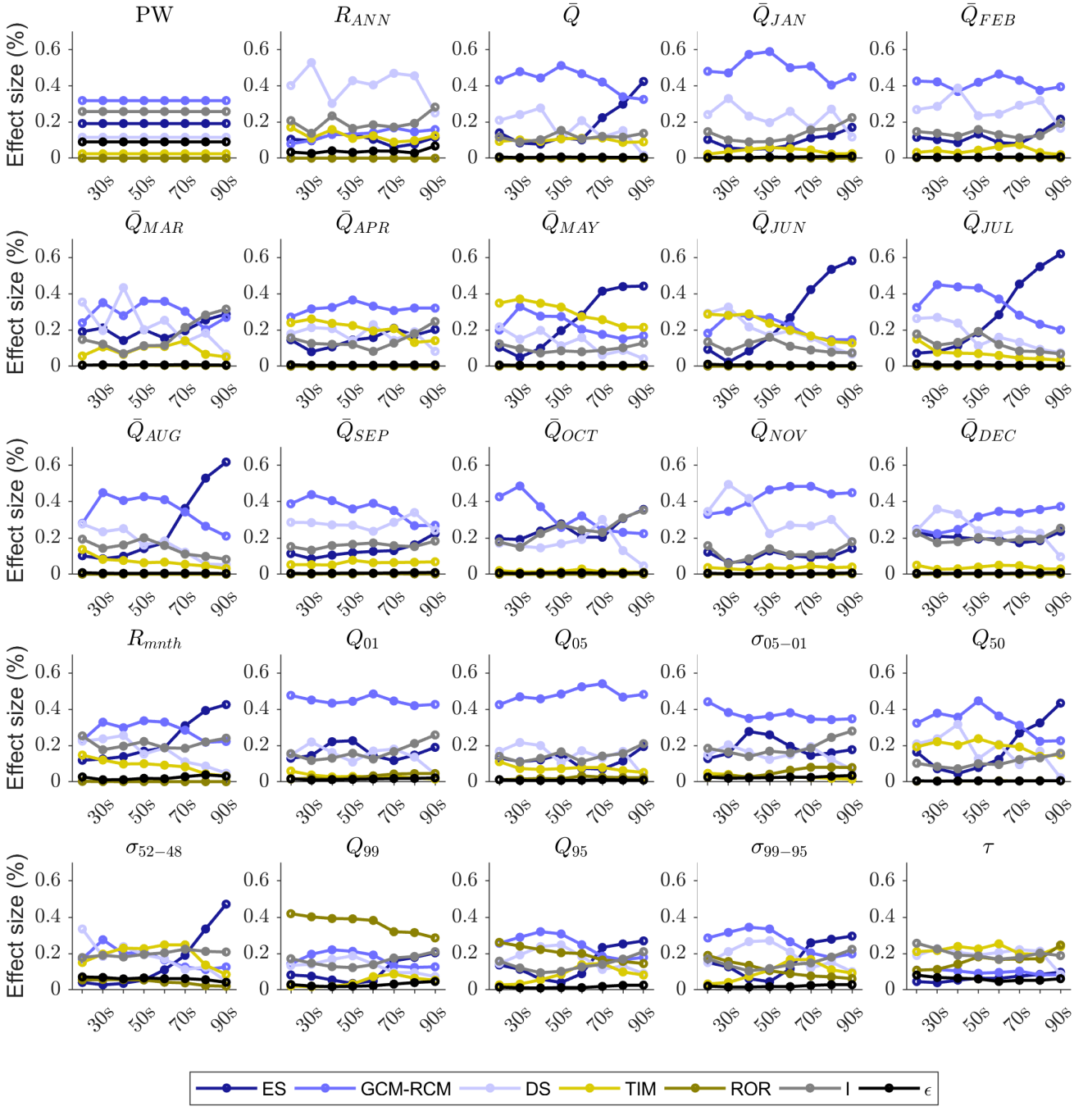

Figure C1. Effect size of all main effects, interactions and remaining error on projected decadal changes in the 25 river discharge signatures for all decades affected by future climate change (2020s to 2090s).

Hydrol. Earth Syst. Sci. Discuss., https://doi.org/10.5194/hess-2018-443
Manuscript under review for journal Hydrol. Earth Syst. Sci.
Discussion started: 5 September 2018

Acknowledgements. This work was supported by a NERC studentship awarded to JDM via the Central England NERC Training Alliance (CENTA).

References

Addor, N., Rössler, O., Köplin, N., Huss, M., Weingartner, R., and Seibert, J.: Robust changes and sources of uncertainty in the projected hydrological regimes of Swiss catchments, Water Resources Research, 50, 7541–7562, https://doi.org/10.1002/2014WR015549, 2014.

Ali, G., Tetzlaff, D., Soulsby, C., McDonnell, J. J., and Capell, R.: A comparison of similarity indices for catchment classification using a cross-regional dataset, Advances in Water Resources, 40, 11–22, https://doi.org/10.1016/j.advwatres.2012.01.008, 2012.

Baraer, M., Mckenzie, J., Mark, B. G., Gordon, R., Bury, J., Condom, T., Gomez, J., Knox, S., and Fortner, S. K.: Contribution of groundwater to the outflow from ungauged glacierized catchments: A multi-site study in the tropical Cordillera Blanca, Peru, Hydrological Processes, 29, 2561–2581, https://doi.org/10.1002/hyp.10386, 2015.

Bartók, B., Wild, M., Folini, D., Lüthi, D., Kotlarski, S., Schär, C., Vautard, R., Jerez, S., and Imecs, Z.: Projected changes in surface solar radiation in CMIP5 global climate models and in EURO-CORDEX regional climate models for Europe, Climate Dynamics, 49, 2665–2683, https://doi.org/10.1007/s00382-016-3471-2, 2017.

Beamer, J. P., Hill, D. F., McGrath, D., Arendt, A., and Kienholz, C.: Hydrologic impacts of changes in climate and glacier extent in the Gulf of Alaska watershed, Water Resources Research, 53, 7502–7520, https://doi.org/10.1002/2016WR020033, 2017.

Beer, C., Porada, P., Ekici, A., and Brakebusch, M.: Effects of short-term variability of meteorological variables on soil temperature in permafrost regions, The Cryosphere, 12, 741–757, https://doi.org/10.5194/tc-12-741-2018, 2018.

Björnsson, H. and Pálsson, F.: Icelandic glaciers, Jökull, 58, 365–386, 2008.

Bliss, A., Hock, R., and Radić, V.: Global response of glacier runoff to twenty-first century climate change, Journal of Geophysical Research, 119, 717–730, https://doi.org/10.1002/2013JF002931, 2014.

Bosshard, T., Carambia, M., Goergen, K., Kotlarski, S., Krahe, P., Zappa, M., and Schär, C.: Quantifying uncertainty sources in an ensemble of hydrological climate-impact projections, Water Resources Research, 49, 1523–1536, https://doi.org/10.1029/2011WR011533, 2013.

Braithwaite, R. J.: Positive degree-day factors for ablation on the Greenland Ice-sheet studied by energy balance modeling, Journal of Glaciology, 41, 153–160, 1995.

Brately, P. and Fox, B. L.: Algorithm 659: Implementing Sobol's quasirandom sequence generator, ACM Transactions on Mathematical Software, 14, 88–100, 1988.

Brock, B. W., Willis, I. C., and Sharp, M. J.: Measurement and parameterisation of albedo variations at Haut Glacier d'Arolla , Switzerland, Journal of Glaciology, 46, 675–688, https://doi.org/10.3189/172756500781832675, 2000.

Bunn, S. E. and Arthington, A. H.: Basic principles and ecological consequences of altered flow regimes for aquatic biodiversity, Environmental Management, 30, 492–507, https://doi.org/10.1007/s00267-002-2737-0, 2002.

Carey, M., Baraer, M., Mark, B. G., French, A., Bury, J., Young, K. R., and McKenzie, J. M.: Toward hydro-social modeling: Merging human variables and the social sciences with climate-glacier runoff models (Santa River, Peru), Journal of Hydrology, 518, 60–70, https://doi.org/10.1016/j.jhydrol.2013.11.006, 2014.

Carvajal, P. E., Anandarajah, G., Mulugetta, Y., and Dessens, O.: Assessing uncertainty of climate change impacts on long-term hydropower generation using the CMIP5 ensemble—the case of Ecuador, Climatic Change, 144, 611–624, https://doi.org/10.1007/s10584-017-2055-4, 2017.

Casper, M. C., Grigoryan, G., Gronz, O., Gutjahr, O., Heinemann, G., Ley, R., and Rock, A.: Analysis of projected hydrological behavior of catchments based on signature indices, Hydrology and Earth System Sciences, 16, 409–421, https://doi.org/10.5194/hess-16-409-2012, 2012.

Chen, J. and Ohmura, A.: On the influence of Alpine glaciers on runoff, IAHS Publication, 193, 117–126, 1990.

Collins, M., Knutti, R., Arblaster, J., Dufresne, J.-L., Fichefet, T., Friedlingstein, P., Gao, X., Gutowski, W., Johns, T., Krinner, G., Shongwe, M., Tebaldi, C., Weaver, A., and Wehner, M.: Long-term Climate Change: Projections, Commitments and Irreversibility, in: Climate Change 2013: The Physical Science Basis. Contribution of Working Group I to the Fifth Assessment Report of the Intergovernmental Panel on Climate Change, edited by Stocker, T., Qin, D., Plattner, G.-K., Tignor, M., Allen, S., Boschung, J., Nauels, A., Xia, Y., Bex, V., and Midgley, P., pp. 1029–1136, Cambridge University Press, Cambridge, United Kingdom and New York, USA, 2013.

Coxon, G., Freer, J., Wagener, T., Odoni, N. A., and Clark, M.: Diagnostic evaluation of multiple hypotheses of hydrological behaviour in a limits-of-acceptability framework for 24 UK catchments, Hydrological Processes, 28, 6135–6150, https://doi.org/10.1002/hyp.10096, 2014.

Duethmann, D., Menz, C., Jiang, T., and Vorogushyn, S.: Projections for headwater catchments of the Tarim River reveal glacier retreat and decreasing surface water availability but uncertainties are large, Environmental Research Letters, 11, 054 024, https://doi.org/10.1088/1748-9326/11/5/054024, 2016.

Euser, T., Winsemius, H. C., Hrachowitz, M., Fenicia, F., Uhlenbrook, S., and Savenije, H. H. G.: A framework to assess the realism of model structures using hydrological signatures, Hydrology and Earth System Sciences, 17, 1893–1912, https://doi.org/10.5194/hess-17-1893-2013, 2013.

Farinotti, D., Usselmann, S., Huss, M., Bauder, A., and Funk, M.: Runoff evolution in the Swiss Alps: projections for selected high-alpine catchments based on ENSEMBLES scenarios, Hydrological Processes, 26, 1909–1924, https://doi.org/10.1002/hyp.8276, 2012.

Finger, D., Pellicciotti, F., Konz, M., Rimkus, S., and Burlando, P.: The value of glacier mass balance, satellite snow cover images, and hourly discharge for improving the performance of a physically based distributed hydrological model, Water Resources Research, 47, W07 519, https://doi.org/10.1029/2010WR009824, 2011.

Flett, V., Maurice, L., Finlayson, A., Black, A. R., MacDonald, A. M., Everest, J., and Kirkbride, M. P.: Meltwater flow through a rapidly deglaciating glacier and foreland catchment system: Virkisjökull, SE Iceland, Hydrology Research, 1, nh2017 205, https://doi.org/10.2166/nh.2017.205, 2017.

Flett, V. T.: Glacier retreat and projected river regime changes in the hydrologically highly-coupled Virkisjökull catchment , SE Iceland, Doctor of philosophy, University of Dundee, 2016.

Fountain, A. G. and Tangborn, W. V.: The Effect of Glaciers on Streamflow Variations, Water Resources Research, 21, 579–586, https://doi.org/10.1029/WR021i004p00579, 1985.

Fyke, J. and Matthews, H. D.: A probabilistic analysis of cumulative carbon emissions and long-term planetary warming, Environmental Research Letters, 10, 115 007, https://doi.org/10.1088/1748-9326/10/11/115007, 2015.

Garee, K., Chen, X., Bao, A., Wang, Y., and Meng, F.: Hydrological Modeling of the Upper Indus Basin: A Case Study from a High-Altitude Glacierized Catchment Hunza, Water, 9, 1–20, https://doi.org/10.3390/w9010017, 2017.

Gaudard, L., Romerio, F., Dalla Valle, F., Gorret, R., Maran, S., Ravazzani, G., Stoffel, M., and Volonterio, M.: Climate change impacts on hydropower in the Swiss and Italian Alps, Science of the Total Environment, 493, 1211–1221, https://doi.org/10.1016/j.scitotenv.2013.10.012, 2014.

Giorgi, F., Jones, C., and Asrar, G. R.: Addressing climate information needs at the regional level: The CORDEX framework, World Meteorological Organization Bulletin, 58, 175–183, 2009.

Giuntoli, I., Vidal, J. P., Prudhomme, C., and Hannah, D. M.: Future hydrological extremes: The uncertainty from multiple global climate and global hydrological models, Earth System Dynamics, 6, 267–285, https://doi.org/10.5194/esd-6-267-2015, 2015.

Gosseling, M.: CORDEX climate trends for Iceland in the 21st century, Tech. rep., Icelandic Meteorological Office, Reykjavik, Iceland, 2017.

Griffiths, J., Keller, V., Morris, D., and Young, A.: Continuous Estimation of River Flows (CERF) : Model Scheme for Representing Rainfall Interception and Soil Moisture. Environment Agency R & D Project W6- 101., Tech. rep., Centre for Ecology and Hydrology, Wallingford, UK, 2006.

Hanzer, F., Helfricht, K., Marke, T., and Strasser, U.: Multilevel spatiotemporal validation of snow/ice mass balance and runoff modeling in glacierized catchments, Cryosphere, 10, 1859–1881, https://doi.org/10.5194/tc-10-1859-2016, 2016.

Hernández-Henríquez, M. A., Sharma, A. R., and Déry, S. J.: Variability and trends in runoff in the rivers of British Columbia's Coast and Insular Mountains, Hydrological Processes, pp. 3269–3282, https://doi.org/10.1002/hyp.11257, 2017.

Hingray, B., Schaefli, B., Mezghani, A., and Hamdi, Y.: Signature-based model calibration for hydrological prediction in mesoscale Alpine catchments, Hydrological Sciences Journal, 55, 1002–1016, https://doi.org/10.1080/02626667.2010.505572, 2010.

Hock, R.: A distributed temperature-index ice- and snowmelt model including potential direct solar radiation, Journal of Glaciology, 45, 101–111, 1999.

Hrachowitz, M., Fovet, O., Ruiz, L., Euser, T., Gharari, S., Nijzink, R., Freer, J., Savenije, H., and Gascuel-Odoux, C.: Process consistency in models: The importance of system signatures, expert knowledge, and process complexity, Water Resources Research, 50, 7445–7469, 2014.

Huss, M. and Hock, R.: Global-scale hydrological response to future glacier mass loss, Nature Climate Change, 8, https://doi.org/10.1038/s41558-017-0049-x, 2018.

Huss, M., Bauder, A., Funk, M., and Hock, R.: Determination of the seasonal mass balance of four Alpine glaciers since 1865, Journal of Geophysical Research: Earth Surface, 113, F01 015, https://doi.org/10.1029/2007JF000803, 2008.

Huss, M., Jouvet, G., Farinotti, D., and Bauder, A.: Future high-mountain hydrology: a new parameterization of glacier retreat, Hydrology and Earth System Sciences, 14, 815–829, https://doi.org/10.5194/hess-14-815-2010, 2010.

Huss, M., Zemp, M., Joerg, P. C., and Salzmann, N.: High uncertainty in 21st century runoff projections from glacierized basins, Journal of Hydrology, 510, 35–48, https://doi.org/10.1016/j.jhydrol.2013.12.017, 2014.

Immerzeel, W. W., Pellicciotti, F., and Bierkens, M. F. P.: Rising river flows throughout the twenty-first century in two Himalayan glacierized watersheds, Nature Geoscience, 6, 742–745, https://doi.org/10.1038/ngeo1896, 2013.

Jakob Themeßl, M., Gobiet, A., and Leuprecht, A.: Empirical-statistical downscaling and error correction of daily precipitation from regional climate models, International Journal of Climatology, 31, 1530–1544, https://doi.org/10.1002/joc.2168, 2011.

Jansson, P., Hock, R., and Schneider, T.: The concept of glacier storage: a review, Journal of Hydrology, 282, 116–129, https://doi.org/10.1016/S0022-1694(03)00258-0, 2003.

Jobst, A. M., Kingston, D. G., Cullen, N. J., and Schmid, J.: Intercomparison of different uncertainty sources in hydrological climate change projections for an alpine catchment (upper Clutha River, New Zealand), Hydrology and Earth System Sciences, 22, 3125–3142, https://doi.org/10.5194/hess-22-3125-2018, 2018.

Jóhannesson, T., Aðalgeirsdóttir, G., Björnsson, H., and Crochet, P.: Effect of climate change on hydrology and hydro-resources in Iceland, Tech. rep., National Energy Authority, Orkugarður, 2007.

Kelleher, C., McGlynn, B., and Wagener, T.: Characterizing and reducing equifinality by constraining a distributed catchment model with regional signatures, local observations, and process understanding, Hydrology and Earth System Sciences Discussions, 21, 3325–3352, https://doi.org/10.5194/hess-2016-642, 2017.

Kiesel, J., Guse, B., Pfannerstill, M., Kakouei, K., Jähnig, S. C., and Fohrer, N.: Improving hydrological model optimization for riverine species, Ecological Indicators, 80, 376–385, https://doi.org/10.1016/j.ecolind.2017.04.032, 2017.

Kobierska, F., Jonas, T., Zappa, M., Bavay, M., Magnusson, J., and Bernasconi, S. M.: Future runoff from a partly glacierized watershed in Central Switzerland: A two-model approach, Advances in Water Resources, 55, 204–214, https://doi.org/10.1016/j.advwatres.2012.07.024, 2013.

Konz, M. and Seibert, J.: On the value of glacier mass balances for hydrological model calibration, Journal of Hydrology, 385, 238–246, https://doi.org/10.1016/j.jhydrol.2010.02.025, 2010.

Laghari., J. R.: Melting glaciers bring energy uncertainty, Nature, 502, 617–618, https://doi.org/10.1038/502617a, 2013.

Li, H., Sheffield, J., and Wood, E. F.: Bias correction of monthly precipitation and temperature fields from Intergovernmental Panel on Climate Change AR4 models using equidistant quantile matching, Journal of Geophysical Research Atmospheres, 115, D10 101, https://doi.org/10.1029/2009JD012882, 2010.

Luce, C. H. and Holden, Z. A.: Declining annual streamflow distributions in the Pacific Northwest United States, 1948-2006, Geophysical Research Letters, 36, L16 401, https://doi.org/10.1029/2009GL039407, 2009.

Lutz, a. F., Immerzeel, W. W., Shrestha, a. B., and Bierkens, M. F. P.: Consistent increase in High Asia's runoff due to increasing glacier melt and precipitation, Nature Climate Change, 4, 587–592, https://doi.org/10.1038/nclimate2237, 2014.

Lutz, A. F., Immerzeel, W. W., Kraaijenbrink, P. D. A., Shrestha, A. B., and Bierkens, M. F. P.: Climate change impacts on the upper indus hydrology: Sources, shifts and extremes, PLoS ONE, 11, https://doi.org/10.1371/journal.pone.0165630, 2016.

Macdonald, A. M., Black, A. R., Dochartaigh, B. É. Ó., Everest, J., Darling, W. G., Flett, V., and Peach, D. W.: Using stable isotopes and continuous meltwater river monitoring to investigate the hydrology of a rapidly retreating Icelandic outlet glacier, Annals of Glaciology, 57, 1–8, https://doi.org/10.1017/aog.2016.22, 2016.

Mackay, J. D., Barrand, N. E., Hannah, D. M., Krause, S., Jackson, C. R., Everest, J., and Aðalgeirsdóttir, G.: Glacio-hydrological melt and run-off modelling: application of a limits of acceptability framework for model comparison and selection, The Cryosphere, 12, 2175–2210, https://doi.org/10.5194/tc-12-2175-2018, 2018.

Magnússon, E., Belart, J. M.-c., Pálsson, F., Ágústsson, H., and Crochet, P.: Geodetic mass balance record with rigorous uncertainty estimates deduced from aerial photographs and lidar data – Case study from Drangajökull ice cap , NW Iceland, The Cryosphere, 10, 159–177, https://doi.org/10.5194/tc-10-159-2016, 2016.

Mankin, J. S., Viviroli, D., Singh, D., Hoekstra, A. Y., and Diffenbaugh, N. S.: The potential for snow to supply human water demand in the present and future, Environmental Research Letters, 10, https://doi.org/10.1088/1748-9326/10/11/114016, 2015.

Marren, P. M.: Magnitude and frequency in proglacial rivers: a geomorphological and sedimentological perspective, Earth-Science Reviews, 70, 203–251, https://doi.org/10.1016/j.earscirev.2004.12.002, 2005.

Matti, B., Dahlke, H. E., Dieppois, B., Lawler, D. M., and Lyon, S. W.: Flood seasonality across Scandinavia - Evidence of a shifting hydrograph?, Hydrological Processes, 31, 4354–4370, https://doi.org/10.1002/hyp.11365, 2017.

McDowell, J. Z. and Hess, J. J.: Accessing adaptation: Multiple stressors on livelihoods in the Bolivian highlands under a changing climate, Global Environmental Change, 22, 342–352, https://doi.org/10.1016/j.gloenvcha.2011.11.002, 2012.

Meresa, H. K. and Romanowicz, R. J.: The critical role of uncertainty in projections of hydrological Extremes, Hydrology and Earth System Sciences Discussions, 21, 4245–4258, https://doi.org/10.5194/hess-2016-645, 2017.

Mora, C., Frazier, A. G., Longman, R. J., Dacks, R. S., Walton, M. M., Tong, E. J., Sanchez, J. J., Kaiser, L. R., Stender, Y. O., Anderson, J. M., Ambrosino, C. M., Fernandez-Silva, I., Giuseffi, L. M., and Giambelluca, T. W.: The projected timing of climate departure from recent variability, Nature, 502, 183, http://dx.doi.org/10.1038/nature12540http://10.0.4.14/nature12540, 2013.

Naiman, R. J., Latterell, J. J., Pettit, N. E., and Olden, J. D.: Flow variability and the biophysical vitality of river systems, Comptes Rendus - Geoscience, 340, 629–643, https://doi.org/10.1016/j.crte.2008.01.002, 2008.

Nawri, N., Pálmason, B., Petersen, G. N., Björnsson, H., and Þorsteinsson, S.: The ICRA atmospheric reanalysis project for Iceland, Tech. rep., Icelandic Meteorological Office, Reykjavík, Iceland, 2017.

Nolin, A. W., Phillippe, J., Jefferson, A., and Lewis, S. L.: Present-day and future contributions of glacier runoff to summertime flows in a Pacific Northwest watershed: Implications for water resources, Water Resources Research, 46, W12 509, https://doi.org/10.1029/2009WR008968, 2010.

Pellicciotti, F., Brock, B., Strasser, U., Burlando, P., Funk, M., and Corripio, J.: An enhanced temperature-index glacier melt model including the shortwave radiation balance : development and testing for Haut Glacier d ' Arolla , Switzerland, 51, 573–587, 2005.

Phillips, E., Finlayson, A., Bradwell, T., Everest, J., and Jones, L.: Structural evolution triggers a dynamic reduction in active glacier length during rapid retreat: Evidence from Falljökull, SE Iceland, Journal of Geophysical Research F: Earth Surface, 119, 2194–2208, https://doi.org/10.1002/2014JF003165, 2014.

Pianosi, F., Beven, K., Freer, J., Hall, J. W., Rougier, J., Stephenson, D. B., and Wagener, T.: Sensitivity analysis of environmental models: A systematic review with practical workflow, Environmental Modelling & Software, 79, 214–232, https://doi.org/https://doi.org/10.1016/j.envsoft.2016.02.008, 2016.

Ponce, V. M.: Engineering hydrology: Principles and practices, http://ponce.sdsu.edu/enghydro/, 2014.

Pool, S., Vis, M. J. P., Knight, R. R., and Seibert, J.: Streamflow characteristics from modelled runoff time series – importance of calibration criteria selection, Hydrology and Earth System Sciences Discussions, 21, 5443–5457, https://doi.org/10.5194/hess-2016-546, 2017.

Ragettli, S., Pellicciotti, F., Bordoy, R., and Immerzeel, W. W.: Sources of uncertainty in modeling the glaciohydrological response of a Karakoram watershed to climate change, Water Resources Research, 49, 6048–6066, https://doi.org/10.1002/wrcr.20450, 2013.

Ragettli, S., Immerzeel, W. W., and Pellicciotti, F.: Contrasting climate change impact on river flows from high-altitude catchments in the Himalayan and Andes Mountains., Proceedings of the National Academy of Sciences of the United States of America, 113, 9222–9227, https://doi.org/10.1073/pnas.1606526113, 2016.

Riggs, G. and Hall, D.: MODIS Snow Products Collection 6 User Guide, Tech. rep., 2015.

Samaniego, L., Kumar, R., Breuer, L., Chamorro, A., Flörke, M., Pechlivanidis, I. G., Schäfer, D., Shah, H., Vetter, T., Wortmann, M., and Zeng, X.: Propagation of forcing and model uncertainties on to hydrological drought characteristics in a multi-model century-long experiment in large river basins, Climatic Change, 141, 435–449, https://doi.org/10.1007/s10584-016-1778-y, 2017.

Sanford, T., Frumhoff, P. C., Luers, A., and Gulledge, J.: The climate policy narrative for a dangerously warming world, Nature Climate Change, 4, 164, http://dx.doi.org/10.1038/nclimate2148http://10.0.4.14/nclimate2148, 2014.

Sawicz, K. A., Kelleher, C., Wagener, T., Troch, P., Sivapalan, M., and Carrillo, G.: Characterizing hydrologic change through catchment classification, Hydrology and Earth System Sciences, 18, 273–285, https://doi.org/10.5194/hess-18-273-2014, 2014.

Schaefli, B.: Snow hydrology signatures for model identification within a limits-of-acceptability approach, Hydrological Processes, 30, 4019–4035, https://doi.org/10.1002/hyp.10972, 2016.

Schaefli, B. and Huss, M.: Integrating point glacier mass balance observations into hydrologic model identification, Hydrology and Earth System Sciences, 15, 1227–1241, https://doi.org/10.5194/hess-15-1227-2011, 2011.

Seibert, J., Vis, M., Kohn, I., Weiler, M., and Stahl, K.: Technical note: Representing glacier geometry changes in a semi-distributed hydrological model, Hydrology and Earth System Sciences, 22, 2211–2224, https://doi.org/10.5194/hess-22-2211-2018, 2018.

Shafii, M. and Tolson, B. A.: Optimizing hydrological consistency by incorporating hydrological signatures intomodel calibration objectives, Water Resources Research, 51, 3796–3814, 2015.

Shea, J. M. and Immerzeel, W. W.: An assessment of basin-scale glaciological and hydrological sensitivities in the Hindu Kush-Himalaya, Annals of Glaciology, 57, 308–318, https://doi.org/10.3189/2016AoG71A073, 2016.

Shea, J. M. and Moore, R. D.: Prediction of spatially distributed regional-scale fields of air temperature and vapor pressure over mountain glaciers, Journal of Geophysical Research Atmospheres, 115, D23 107, https://doi.org/10.1029/2010JD014351, 2010.

Singh, S., Kumar, R., Bhardwaj, A., Sam, L., Shekhar, M., Singh, A., Kumar, R., and Gupta, A.: Changing climate and glacio-hydrology in Indian Himalayan Region: A review, Wiley Interdisciplinary Reviews: Climate Change, 7, 393–410, https://doi.org/10.1002/wcc.393, 2016.

Stewart, I. T., Ficklin, D. L., Carrillo, C. A., and McIntosh, R.: 21st century increases in the likelihood of extreme hydrologic conditions for the mountainous basins of the Southwestern United States, Journal of Hydrology, 529, 340–353, https://doi.org/10.1016/j.jhydrol.2015.07.043, 2015.

Stoffel, M., Wyżga, B., and Marston, R. A.: Floods in mountain environments: A synthesis, Geomorphology, 272, 1–9, https://doi.org/https://doi.org/10.1016/j.geomorph.2016.07.008, 2016.

Tabachnick, B. G. and Fidell, L. S.: Using Multivariate Statistics Sixth Edition, Pearson Education Limited, Essex, United Kingdom, sixth edn., 2014.

Taylor, K. E., Stouffer, R. J., and Meehl, G. a.: An Overview of CMIP5 and the Experiment Design, Bulletin of the American Meteorological Society, 93, 485–498, https://doi.org/10.1175/BAMS-D-11-00094.1, 2012.

Teutschbein, C., Grabs, T., Karlsen, R. H., Laudon, H., and Bishop, K.: Hydrological response to changing climate conditions: Spatial streamflow variability in the boreal region, Water Resources Research, 51, 9425–9446, https://doi.org/10.1002/2015WR017337, 2015.

Thorsteinsson, T. and Björnsson, H.: Climate Change and Energy Systems: Impacts, Risks and Adaptation in the Nordic and Baltic countries, Tech. rep., Nordic Council of Ministers, Copenhagen, 2012.

Vaughan, D., Comiso, J., Allison, I., Carrasco, J., Kaser, G., Kwok, R., Mote, P., Murray, T., Paul, F., Ren, J., Rignot, E., Solomina, O., Steffen, K., and Zhang, T.: Observations: Cryosphere, in: Climate Change 2013: The Physical Science Basis. Contribution of Working Group I to the Fifth Assessment Report of the Intergovernmental Panel on Climate Change, edited by Stocker, T., Qin, D., Plattner, G.-K., Tignor, M., Allen, S., Boschung, J., Nauels, A., Xia, Y., Bex, V., and Midgley, P., pp. 358–359, Cambridge University Press, Cambridge, United Kingdom and New York, NY, USA, 2013.

Vetter, T., Huang, S., Aich, V., Yang, T., Wang, X., Krysanova, V., and Hattermann, F.: Multi-model climate impact assessment and intercomparison for three large-scale river basins on three continents, Earth System Dynamics, 6, 17–43, https://doi.org/10.5194/esd-6-17-2015, 2015.

Vetter, T., Reinhardt, J., Flörke, M., van Griensven, A., Hattermann, F., Huang, S., Koch, H., Pechlivanidis, I. G., Plötner, S., Seidou, O., Su, B., Vervoort, R. W., and Krysanova, V.: Evaluation of sources of uncertainty in projected hydrological changes under climate change in 12 large-scale river basins, Climatic Change, 141, 419–433, https://doi.org/10.1007/s10584-016-1794-y, 2017.

Viviroli, D. and Weingartner, R.: The hydrological significance of mountains: from regional to global scale, Hydrology and Earth System Sciences, 8, 1016–1029, https://doi.org/10.5194/hess-8-1017-2004, 2004.

Viviroli, D., Dürr, H. H., Messerli, B., Meybeck, M., and Weingartner, R.: Mountains of the world, water towers for humanity: Typology, mapping, and global significance, Water Resources Research, 43, 1–13, https://doi.org/10.1029/2006WR005653, 2007.

von Storch, H. and Zwiers, F. W.: Statistical Analysis in Climate Research, Cambridge University Press, Cambridge, United Kingdom, 1999.

Wijngaard, R. R., Lutz, A. F., Nepal, S., Khanal, S., Pradhananga, S., Shrestha, A. B., and Immerzeel, W. W.: Future changes in hydro-climatic extremes in the Upper Indus, Ganges, and Brahmaputra River basins, PLOS ONE, 12, e0190 224, https://doi.org/10.1371/journal.pone.0190224, http://dx.plos.org/10.1371/journal.pone.0190224, 2017.

Willis, I.: 168: Hydrology of Glacierized Basins, Encyclopedia of Hydrological Sciences: Part 14. Snow and Glacier Hydrology, 2005.

Yadav, M., Wagener, T., and Gupta, H.: Regionalization of constraints on expected watershed response behavior for improved predictions in ungauged basins, Advances in Water Resources, 30, 1756–1774, https://doi.org/10.1016/j.advwatres.2007.01.005, 2007.

Yuan, F., Zhao, C., Jiang, Y., Ren, L., Shan, H., Zhang, L., Zhu, Y., Chen, T., Jiang, S., Yang, X., and Shen, H.: Evaluation on uncertainty sources in projecting hydrological changes over the Xijiang River basin in South China, Journal of Hydrology, 554, 434–450, https://doi.org/10.1016/j.jhydrol.2017.08.034, 2017.

Zemp, M., Frey, H., Gärtner-Roer, I., Nussbaumer, S. U., Hoelzle, M., Paul, F., Haeberli, W., Denzinger, F., Ahlstrøm, A. P., Anderson, B., Bajracharya, S., Baroni, C., Braun, L. N., Càceres, B. E., Casassa, G., Cobos, G., Dàvila, L. R., Delgado Granados, H., Demuth, M. N., Espizua, L., Fischer, A., Fujita, K., Gadek, B., Ghazanfar, A., Hagen, J. O., Holmlund, P., Karimi, N., Li, Z., Pelto, M., Pitte, P., Popovnin, V. V., Portocarrero, C. A., Prinz, R., Sangewar, C. V., Severskiy, I., Sigurdsson, O., Soruco, A., Usubaliev, R., and Vincent, C.: Historically unprecedented global glacier decline in the early 21st century, Journal of Glaciology, 61, 745–762, https://doi.org/10.3189/2015JoG15J017, 2015.